

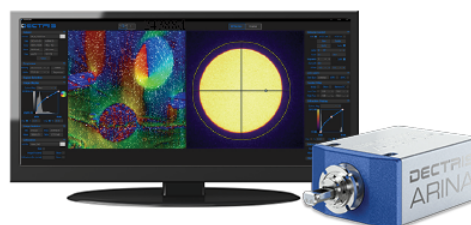
# Novel Insights Into the Architecture of Macro and Microstructures in Cattle Ossa Cordis

Mohamed A M Alsafy, Samir A A El-Gendy, Brian Atkinson, Craig J Sturrock, Basma M Kamal, Aziza Alibhai, Hanan H Abd-Elhafeez, Soha Soliman, Ahmed M Rashwan, Karam Roshdy, Catrin S Rutland

DECTRIS

**ARINA with NOVENA**




**Fast 4D STEM**



DECTRIS NOVENA and CoM analysis of a magnetic sample.

Sample courtesy: Dr. Christian Liebscher, Max-Planck-Institut für Eisenforschung GmbH.  
Experiment courtesy: Dr. Mingjun Wu and Dr. Philipp Hein, Friedrich-Alexander-Universität, Erlangen-Nürnberg.

# Novel Insights Into the Architecture of Macro and Microstructures in Cattle *Ossa Cordis*

Mohamed A.M. Alsafy<sup>1</sup> , Samir A.A. El-Gendy<sup>1</sup> , Brian Atkinson<sup>2</sup>, Craig J. Sturrock<sup>2</sup>,  
Basma M. Kamal<sup>3</sup>, Aziza Alibhai<sup>4</sup>, Hanan H. Abd-Elhafeez<sup>5</sup>, Soha Soliman<sup>6</sup>, Ahmed M. Rashwan<sup>7</sup> ,  
Karam Roshdy<sup>8</sup>, and Catrin S. Rutland<sup>4,\*</sup> 

<sup>1</sup>Department of Anatomy and Embryology, Faculty of Veterinary Medicine, Alexandria University, Abis 10th, Alexandria, PO 21944, Egypt

<sup>2</sup>Hounsfield Facility, School of Biosciences, University of Nottingham, College Road, Sutton Bonington, Leicestershire LE12 5RD, UK

<sup>3</sup>Department of Anatomy and Embryology, Faculty of Veterinary Medicine, University of Sadat City, Sadat City 6010230, Egypt

<sup>4</sup>School of Veterinary Medicine and Science, Faculty of Medicine and Health Science, University of Nottingham, College Road, Sutton Bonington, Leicestershire LE12 5RD, UK

<sup>5</sup>Department of Cell and Tissues, Faculty of Veterinary Medicine, Assiut University, Assiut 71526, Egypt

<sup>6</sup>Department of Histology, Faculty of Veterinary Medicine, South Valley University, Qena 83523, Egypt

<sup>7</sup>Department of Anatomy and Embryology, Faculty of Veterinary Medicine, Damanhour University, Al Gomhouria St, Scientific Campus, Damanhour 22511, Egypt

<sup>8</sup>Department of Histology and Cytology, Faculty of Veterinary Medicine, Alexandria University, Abis 10th, Alexandria, PO 21944, Egypt

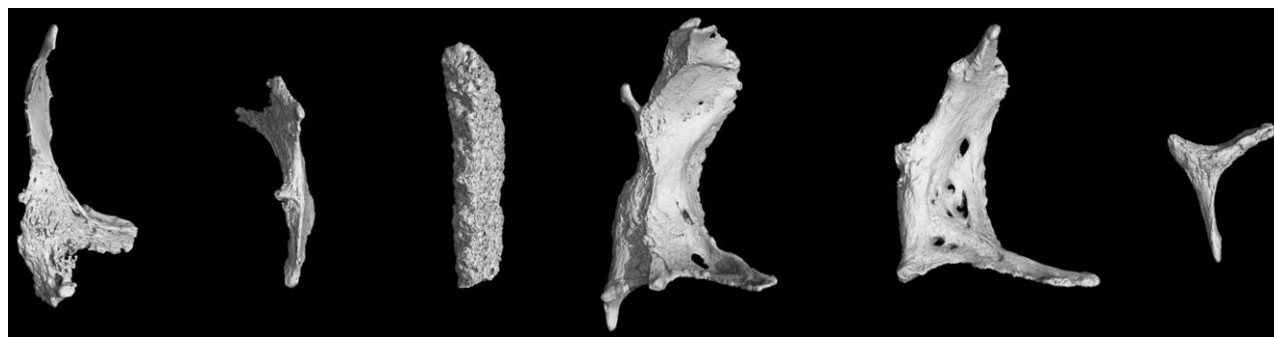
\*Corresponding author: Catrin Rutland, E-mail: [catrin.rutland@nottingham.ac.uk](mailto:catrin.rutland@nottingham.ac.uk)

## Abstract

*Ossa cordis*, bones located within the heart trigones, are often classified as heterotopic or ectopic bones. Despite their high prevalence in cattle and some other bovids, little is known about their structure or development. Scanning electron microscopy, X-ray microtomography, gross dissections, and measurements showed the anatomical locations, prevalence, shapes, and measurements of the cardiac bones in both Egyptian Baladi cattle and Holstein-Friesians. All cattle ( $n = 12$ ) had an *Ossa cordis dextrum* (average =  $50.70 \times 20.91 \times 5.40$  mm). Additionally, 80% Egyptian Baladi and 57% Holstein-Friesian had a smaller *Ossa cordis sinistrum* (average =  $24.94 \times 12.75 \times 4.12$  mm). Egyptian Baladi *Ossa cordis* were smaller than observed in Holstein-Friesians. Energy-dispersive X-ray analysis showed the elemental constitution (carbon, oxygen, calcium, nitrogen, phosphorus, sodium, and magnesium) of *Ossa cordis* and *Cartilago cordis*. These imaging techniques, plus four histological stains (hematoxylin and eosin, Crossman's trichrome, Alcian blue with Van Gieson, and Sirius Red) and microscopy, demonstrated osteoblasts, osteocytes, osteoclasts, astrocytes, blood vessels, bone marrow, lamellar and woven bone, cortical bone, trabeculations with pores and canaliculi, and fibrous components including collagen in the *Ossa cordis dextrum* and *sinistrum*. Hyaline cartilage and fibrocartilage (chondrocytes and cartilage matrix) were found within and surrounding the *Ossa cordis*. These findings were additionally compared against other cattle breeds and species.

**Key words:** computed tomography, energy-dispersive X-ray analysis, heart, heterotopic bone, microscopy

## Graphical Abstract



Received: January 5, 2024. Revised: March 22, 2024. Accepted: April 7, 2024

© The Author(s) 2024. Published by Oxford University Press on behalf of the Microscopy Society of America.

This is an Open Access article distributed under the terms of the Creative Commons Attribution License (<https://creativecommons.org/licenses/by/4.0/>), which permits unrestricted reuse, distribution, and reproduction in any medium, provided the original work is properly cited.

## Introduction

Within the cardiac skeleton, the fibrous trigones are located between the aorta and the atrioventricular openings, and together with the aortic fibrous, it forms the central fibrous body. The trigones in most species are composed of dense connective tissue and can contain fibrocartilage and hyaline cartilage (*Cartilago cordis*) and even bone (*Ossa cordis*) in a limited number of species, as described in detail previously (Best et al., 2022). In brief, buffalo, camel, cat, cattle, chimpanzee, antelope and deer, dog, elephant, giraffe, goat, horse, otter, sea lion, and sheep all have documented *Ossa cordis* (David, 1937; Barasa & Gobetto, 1957; James, 1965; Frink & Merrick, 1974; Long & Smart, 1976; Habermehl & Schmack, 1986; Egerbacher et al., 2000; Mohammadpour, 2007; Matsuda et al., 2010; Balah et al., 2014; Daghash & Farghali, 2017; Vazquez et al., 2019; Moittie et al., 2020; Maguigad & Balagan, 2021; de Almeida Lima Massari et al., 2022; Yoshida et al., 2022; El-Gendy et al., 2023). Bone cells, although not a full *Ossa cordis*, have been observed in the human fulcrum (Tohno et al., 2007; Trainini et al., 2021). When more than one *Ossa cordis* is present, they are differentiated in the right-sided, often larger *Ossa cordis dextrum*, and the left-sided, usually smaller *Ossa cordis sinistrum* (Best et al., 2022).

*Ossa cordis* are often classified as heterotopic (abnormal growth of bone in the nonskeletal tissues) or ectopic bones (ossification of tissues outside their usual origins) (Nasoori, 2020). Although frequently described as heterotopic or ectopic, *Ossa cordis* are present in several cattle breeds and water buffalo, within healthy and diseased hearts. They are also common in other species of the Bovidae family, within the order Artiodactyla including sheep, goats, and antelope. The closely related Cervidae, Giraffidae, and Camelidae families, within the Artiodactyla order also contain species with *Ossa cordis* (Best et al., 2022). The presence of ossification within the diseased heart has also been recorded in people (Kuzela et al., 1977; Steiner et al., 2007), in dogs (James & Drake, 1968), and in some chimpanzees (Moittie et al., 2020). Therefore, although present in healthy hearts of some species, and diseased hearts in others, it is perhaps the limited number of species in which the *Ossa cordis* is present that makes this bone heterotopic or ectopic.

Many techniques have been used to investigate *Ossa cordis* over the years, with most publications using histological sections, X-rays, and computed tomography (CT) such as in the buffalo, lamb, and one-humped camel (Daghash & Farghali, 2017; Maguigad & Balagan, 2021; de Almeida Lima Massari et al., 2022; El-Gendy et al., 2023). Only one publication has used microtomography (microCT) to investigate the microstructure of *Ossa cordis*, and that was in chimpanzees (Moittie et al., 2020). Energy-dispersive X-ray analysis (EDX), an X-ray technique used to identify the elemental composition of materials, has not previously been used to analyze *Ossa cordis* in any species. Scanning electron microscopy (SEM) and high-resolution X-ray microCT have been used generally to evaluate bone architecture and details of the trabecular (cancellous) surfaces and cortical (compact) bone morphology in animals and people (Chappard et al., 2011; Kytir et al., 2012; Witkowska et al., 2014; Keane et al., 2017), but to date, microCT has only been used to investigate chimpanzee *Ossa cordis* (Moittie et al., 2020) and SEM has not been used in any species. It has been noted that the

biomechanical behavior of trabecular bone depends not only on its microarchitecture but also on mineral density distribution (Bouxsein et al., 2010), hence why using this technique would give better insight into *Ossa cordis*. Despite these advances in technology and knowledge regarding bone in general, the *Ossa cordis* of cattle, or most other species with these bones, have not been investigated using these methods.

In the present research, two key cattle breeds were investigated. The Egyptian Baladi cattle represents one of the few original taurine breeds remaining in the original domestication area of *Bos taurus*, the Nile Valley (Upper Egypt). Apart from its evolutionary relevance, the breed is well adapted and integrated into the traditional family farming systems, with great potential for local sustainable rural development as a meat, draft, and dairy breed. The second breed investigated was the Holstein-Friesian, a European breed originating from the Netherlands, an essential dairy breed with the largest number of individuals of any breed, spread throughout 165 countries (United Nations, 2023). Cattle are ungulates in the Artiodactyla order, a member of the Bovidae family, in the subfamily Bovinae, and the genus *Bos primigenius* refers to all cattle. Cattle are thought to have become domesticated during the early Neolithic era (Lenstra et al., 1999; Daetwyler et al., 2014; Zhang et al., 2020; Rutland, 2021). Following domestication of the Bovini species (taurine cattle, zebu, yak, river buffalo, and swamp buffalo) in the early Holocene (ca. 10,000 BCE), they have played a number of significant roles in the development of human civilization and remain key economic factors throughout the world, especially in terms of food security (Molina-Flores et al., 2020).

Given the lack of knowledge relating to *Ossa cordis* in general, and the presence of this structure in cattle, the aims of our investigations were to explore the macro and microstructures of *Ossa cordis* in domesticated cattle. Gross morphology and measurements were taken, and CT, microCT, histological staining alongside light microscopy, SEM, and SEM-EDX were used to describe the anatomical location, prevalence, gross and microscopic structure, and element composition of the *Ossa cordis* and associated cartilaginous tissue.

## Materials and Methods

### Specimens and Ethics

Two breeds of cattle were used. All were adult (2–3 years), healthy animals, five male Egyptian Baladi cattle, and seven Holstein-Friesian. None had a history of clinical cardiac abnormalities; they were slaughtered by a professional veterinary surgeon and were not slaughtered for research purposes. This research was approved by the Animal Welfare and Ethics Committees, in the Faculty of Veterinary Medicine, Alexandria University (No. 02/13/2023/02/01/212), and the University of Nottingham, School of Veterinary Medicine and Science Ethics Committee (No. 1843 160905), in accordance with institutional, national, and international guidelines. The hearts were dissected out at the slaughterhouse, placed on ice, and immediately transferred to the laboratory. The fresh hearts were examined and imaged within 2 h of death in order to reduce any potential postmortem variations. Immediately following CT imaging, the specimens were processed for histology. The bones used for microCT analysis and gross morphological imaging were dissected from the soft tissue and then scanned.

### Gross Analysis and X-ray microCT

Following bone extraction, the *Ossa cordis dextrum* and *sinistrum* underwent basic gross morphology photography and precision caliper measurements (length, depth, and breadth) to a two-decimal place level. Each *Ossa cordis* was then secured in thin sheets of X-ray transparent polyethylene packing foam within plastic specimen jars. A Phoenix vltomel x m (Waygate Technologies GmbH, Wunstorf, Germany), X-ray microCT system was used set at an X-ray tube energy and current of 115 kV and 220  $\mu$ A, respectively. Scans were made at a resolution of 60  $\mu$ m. Each scan acquired 2,400 projection images over a 360° rotation of the sample using a detector exposure time of 500 ms in “FAST scan mode” (i.e., continuous rotation and no projection image integration). Projection image data were reconstructed in datoslx software (Waygate Technologies, Wunstorf, Germany) and exported as a three-dimensional (3D) volume file. Higher-resolution scans were conducted on dissected regions at 24  $\mu$ m to reveal the microstructure of the dense objects. High-resolution scans were acquired at 82 kV, 250  $\mu$ A, 400 ms detector timing, and 2,400 projection images with each image being the integration of two images to reduce noise. X-ray CT image data were visualized using VGStudioMAX v3.0 Software (Volume Graphics GmbH, Heidelberg, Germany). The high-density objects were digitally segmented from the 3D volumetric data based on their higher X-ray attenuation values in the images (brighter color) and exported as image stacks. microCT was conducted at The Hounsfield Facility, University of Nottingham.

### CT (3D Render Volume CT; 128-Slice Multidetector CT Scanning)

Five hearts were positioned on their right-side surfaces for each scan. The hearts were secured in a foam material to avoid any movement that would interfere with image quality. The CT X-ray examinations were performed on an AMDCT scanner with 128 detectors (Aquilion; Toshiba Medical Systems, Tokyo, Japan), with a rotation time of 300 ms, and a slice collimation of 128  $\times$  0.6 mm<sup>2</sup>, using a continuous helical scan MinDose technique. After obtaining a preliminary image to determine the 3D-CTA scan range, serial cross section scans from the apex to the base of each heart were conducted using a slide thickness of 1 mm with 1.3 mm intervals, with the following soft window settings: 240 mA, 130 kV, width.342, and length.52, and the sections did not overlap but several scans were undertaken. To obtain sagittal sections using the soft tissue window, the scans were conducted at the level of the interventricular septum and about 20 scans were made at 1.8 mm intervals at a thickness of 8 mm, with setting set at 240 mA, 130 kV, width.342, and length.52. The CT image reconstruction was undertaken using the optimal reconstruction parameters for hearts. Initially, a set of cross-sectional tomography slices were constructed individually; then, the images were stacked together sequentially to obtain a 3D image model of each heart. The reconstruction algorithm was used within the Octopus software and then converted into a DICOM format producing three reconstruction images: ghost (black and white) render, color render (red in color), and an angiograph, which was translucent blue in color (Dankowski et al., 2014). The CT images were analyzed using the ImageJ 1.53 k application (National Institutes of Health, USA) to measure the *Ossa cordis* using the previously

described method (Witkowska et al., 2014; Moittie et al., 2020; El-Gendy et al., 2023).

### Scanning Electron Microscopy

The samples of cross sections containing *Ossa cordis* were fixed in a buffer solution containing 2% formaldehyde, 1.25% glutaraldehyde, and 0.1 M sodium cacodylate at pH 7.2 at 4°C. After fixation, the samples were washed in 0.1 M sodium cacodylate containing 5% sucrose, processed through tannic acid, and finally dehydrated in increasing grades of ethanol (15 min each in 50, 70, 80, 90, 95, and 100% ethanol). The samples were then dried in carbon dioxide, attached to stubs with colloidal carbon, and coated with gold-palladium in a sputtering device. The specimens were imaged with a JEOL JSM-IT200 scanning electron microscope at 15 kV at the Electron Microscope Unit, Faculty of Science, Alexandria University according to methods described previously (Gebert & Preiss, 1998; El-Bakary et al., 2023).

### SEM-EDX Measurements

EDX, an X-ray technique, is used to identify the elemental composition of materials. As  $n=2$  *Ossa cordis dextrum* trabecular bone and cartilaginous tissue surrounding the cortical bone were used, and counts were below 10,000, qualitative descriptions of the elements were applied. They were analyzed using a JEOL JSM-IT200 scanning electron microscope at 20 kV, using the integrated manufacturer's software SMILE VIEW™ Lab. The sample distance from the detector was 10 mm, with a real time of 30.97 s and a dead time of 3.00%. The EDX spectrometer and software are based at the Science Faculty, Alexandria University, Egypt.

### Histological Staining and Microscopy

The *Ossa cordis dextrum* and *sinistrum* from three hearts, as observed following CT scans, were processed for histological analysis. The 1 cm<sup>3</sup> heart samples containing the *Ossa cordis* were manually dissected, fixed in 10% buffered neutral formalin and decalcified. The samples were decalcified using 10% ethylenediaminetetraacetic acid (EDTA) in 0.1 M Tris/HCl buffer, pH 7.4, for 6 days, with solution changes every 2 days (Abd-Elhafeez et al., 2021). Thereafter, the specimens were dehydrated in ethanol, cleared in xylene, and then embedded in paraffin wax. Serial sections 5–7  $\mu$ m thick were prepared using a Reichert Leica RM 2125 Microtome (Germany) and mounted on glass slides. The sections were stained with hematoxylin and eosin (H&E) using a previously published method (Gamble, 2008). Other sections were stained with either Crossman's trichrome or Alcian blue pH 2.5 with Van Gieson stain (Suvarna et al., 2018). Sections were also stained with Sirius Red (Junqueira et al., 1979), Red F3B Sirius 0.5 g (Sigma-Aldrich Cat No 36-554-08 Direct Red 80) in 500 mL picric acid saturated aqueous solution for 1 h followed by two acidic acid washes (5 mL glacial acetic acid in 1 L of distilled water). These stained tissue sections were inspected using an Olympus CX31 microscope, and the images were recorded using a Canon digital camera.





**Fig. 1.** Gross anatomy. (a,b) *Ossa cordis dextrum* from the Holstein-Friesian and Egyptian Baladi cattle, respectively. (c,d) *Ossa cordis sinistram* from the Holstein-Friesian and Egyptian Baladi cattle, respectively. Scale bars represent 1 cm.

## Results

### Measurements, Location, Prevalence, and Shape of *Ossa Cordis* Using Gross Morphology, CT, and microCT

Gross morphological images and precision caliper measurements (Fig. 1; Table 1) were used to assess the shapes and sizes of the *Ossa cordis dextrum* and *sinistram*. In addition, microCT was used to show shape and internal morphology (Figs. 2–5). Three windows of 3D rendered volume were also used to detect *Ossa cordis*, black and white, color, and blue angiography without contrast media window (Fig. 6). These also showed the locations, sizes, and shapes of the *Ossa cordis*.

### Measurements, Location, Prevalence, and Shape of *Ossa Cordis Dextrum*

CT and microCT showed that the *Ossa cordis dextrum* varied in shape from oval to mainly elongated quadrilateral or rectangular with a pointed caudoventral end and a rounded cranial end. The CT sequential cross sections of the *Ossa cordis dextrum* confirmed they were varied in shape, with a short ovoid shape at the caudal end of the bone, continuing as a long avoid or rectangular shape in the middle part of the bone, while the cranial ends of the bones were generally a short rectangular shape (Figs. 1–3, 7–9; Supplementary Video 1). *Ossa cordis dextrum* were located on the right side of the heart at the upper part of the interventricular septum, land marker externally as the cranial end of the bone at the level of the caudal part of conus arteriosus and the caudal end of the bone was located at the corresponding upper part of the right interventricular subsinusal groove, about 1–1.5 cm under the coronary groove (Fig. 9).

On average, the *Ossa cordis dextrum* in the present study ( $n = 12$ ) were 50.70 mm long, 20.91 mm wide at their widest part, and 5.05 mm wide at the thinnest part, 5.40 mm in depth at the thickest part, and 2.83 mm in depth at the thinnest part, with a prevalence of 100% in both Egyptian Baladi cattle and

Holstein-Friesian cattle hearts. The full ranges, averages, and values for both Egyptian Baladi cattle and Holstein-Friesian cattle are exhibited in Table 1. The Egyptian Baladi *Ossa cordis dextrum* were generally smaller than the Holstein-Friesian cattle (for all measurements and  $p$  values, please see Table 1). Cartilage linking the *Ossa cordis dextrum* and *sinistram* was not observed using any of the methods used in this study.

### Measurements, Location, Prevalence, and Shape of *Ossa Cordis Sinistram*

As shown by CT and microCT, the *Ossa cordis sinistram* also varied in shape from oval to mainly triangular as also confirmed in the sequential cross sections, microCT, and gross morphology photographs (Figs. 1, 4, 5, 8; Supplementary Video 2). The caudal end was generally wider, while the cranial, narrow end was more pointed, but this was not the case for every *Ossa cordis*. The *Ossa cordis sinistram* were located under the beginning of the left coronary artery and in some specimens appeared to be adhered to the aortic wall (Fig. 3).

The *Ossa cordis sinistram* were smaller than the *Ossa cordis dextrum*, with a prevalence of 80% in Egyptian Baladi cattle hearts and 57% in the Holstein-Friesian hearts. On average ( $n = 8$ ), they measured 24.94 mm long, 12.75 mm in width at the widest part, 2.75 mm in width at the narrowest part, 4.12 mm in depth at the thickest part, and 1.78 mm in depth at the thinnest part. The ranges and averages, for both the Egyptian Baladi cattle and Holstein-Friesian *Ossa cordis*, are presented in Table 1. The Egyptian Baladi *Ossa cordis sinistram* were generally smaller than those observed in the Holstein-Friesian cattle (for all measurements and  $p$  values, please see Table 1). The *Ossa cordis sinistram* were also smaller than *Ossa cordis dextrum* in both breeds (Table 1).

### microCT, SEM, and SEM-EDX Visualization of the *Ossa Cordis*

Both microCT and SEM detection of the *Ossa cordis dextrum* and *sinistram* showed trabecular bone in the center of the

**Table 1.** Measurements of *Ossa Cordis*.

	Length (mm)	Width—Widest Part (mm)	Width—Narrowest Part (mm)	Depth—Thickest Part (mm)	Depth—Thinnest Part (mm)
Egyptian Baladi cattle, dextrum ( <i>n</i> = 5)	39.00–50.00 (43.68)	8.20–18.80 (12.59)	2.60–3.74 (3.31)	3.17–4.00 (3.67)	1.50–4.00 (3.34)
Egyptian Baladi cattle, sinistrum ( <i>n</i> = 4) <sup>a</sup>	13.00–24.50 (18.63)	8.40–9.30 (9.00)	1.10–1.40 (1.25)	3.50–4.40 (4.00)	1.50–2.00 (1.83)
Holstein, dextrum ( <i>n</i> = 7)	45.00–70.00 (55.71)	10.00–47.00 (26.86)	4.00–10.00 (6.29)	4.50–11.00 (6.63)	1.00–6.00 (2.47)
Holstein, sinistrum ( <i>n</i> = 4) <sup>a</sup>	17.00–45.00 (31.25)	7.00–22.00 (16.50)	3.00–5.00 (4.25)	2.10–8.08 (4.21)	0.85–2.66 (1.75)
Average (all dextrum <i>n</i> = 12)	50.70	20.91	5.05	5.40	2.83
Average (all sinistrum <i>n</i> = 8)	24.94	12.75	2.75	4.12	1.78
<b>Statistical outcomes (<i>p</i> value)</b>					
Egyptian Baladi cattle, dextrum ( <i>n</i> = 5) versus Egyptian Baladi cattle, sinistrum ( <i>n</i> = 4)	<b>0.0001</b>	0.133	<b>0.0001</b>	0.307	0.055
Holstein, dextrum ( <i>n</i> = 7) versus Holstein sinistrum ( <i>n</i> = 4)	<b>0.01</b>	0.186	0.12	0.145	0.471
Egyptian Baladi cattle, dextrum ( <i>n</i> = 5) versus Holstein, dextrum ( <i>n</i> = 7)	<b>0.044</b>	<b>0.03</b>	<b>0.011</b>	<b>0.011</b>	<b>0.321</b>
Egyptian Baladi cattle, sinistrum ( <i>n</i> = 4) versus Holstein, sinistrum ( <i>n</i> = 4)	0.095	0.066	<b>0.008</b>	0.906	0.859

Range smallest to largest (average).

<sup>a</sup>Four out of five Egyptian Baladi cattle had both bones; four out of seven Holstein cattle had both bones. Prevalence = dextrum Egyptian Baladi cattle 100%, Holstein 100%; sinistrum Egyptian Baladi cattle 80%, and Holstein 57%. Statistical tests = Levene's test for equality of variances followed by *t* test for equality of means, *p* < 0.05 showed statistically significant difference, marked in bold font.

*Ossa cordis*, surrounded by cortical bone, which had intermittent cartilage covering it (Figs. 2–5, 10; Supplementary Videos 1, 2). There were irregular pores on the external surface of the cortical bone (Figs. 2–5, 10; Supplementary Videos 1, 2). SEM also showed that the irregularly shaped external surface of the cartilage was characterized by dome-shaped projections and elliptical pores. The trabecular bone had trabecular projections, which were flat and connected to each other and contained large circular large pores visible at higher magnifications (Fig. 10). The trabeculations also contained microridges in irregular directions, mineral decomposition at the bony plate, in addition to many pores from canaliculi. The trabeculated bone also contained rounded balls of bone marrow between the trabecular plates (Fig. 10).

Microelemental pictures of the *Ossa cordis* specimens from the energy-dispersive X-ray spectra with an accelerating voltage (20 keV) were also recorded. Two areas were assessed, the trabecular bone within the *Ossa cordis dextrum* (Fig. 11) and the cartilaginous tissue surrounding the *Ossa cordis dextrum* (Fig. 12). The following elements were detected in *Ossa cordis* cartilaginous covering and in the trabeculations: carbon, oxygen, calcium, nitrogen, phosphorus, and sodium, whereas magnesium was only present in the trabeculations (Figs. 11, 12).

## Histological Analysis

### Histological Characterization Using H&E

The histological examinations showed that the larger *Ossa cordis dextrum* in each heart had hyaline cartilage, with chondrocytes, surrounding the cortical bone of the *Ossa cordis dextrum* and *sinistrum*. Sites displaying ossification of the cartilage were also observed (overview Fig. 13). Inside the cortical bone were bone trabeculations containing numerous astrocytes. Between trabeculations, bone marrow was present (Fig. 13).

The *Ossa cordis dextrum* comprised trabecular bone tissue, and the outer surface was covered by hyaline cartilage (Fig. 14a). Hyaline cartilage consisted of chondrocytes located inside a lacuna and surrounded by a cartilage matrix (Fig. 14b). Fibrocartilage connected the hyaline cartilage and the outer fibrous tissue (Fig. 14c). Intracartilaginous ossification was recognized via bone deposition inside the cartilage lacuna (Fig. 14d). The formation of bone tissue also occurred at the surface of the hyaline cartilage. Osteocytes are embedded within the bone matrix and located inside a lacuna (Fig. 14e). Several types of bone cells were identified. Osteoclasts were multinucleated cells and had deep acidophilic cytoplasm (Figs. 15a, 15c, 15d). Osteoblasts occurred on the surface of the bone trabeculae (Fig. 15b). Hematopoietic tissue was observed in the bone marrow (Fig. 15e).

### Histological Characterization Using Sirius Red Stain

Sirius Red stain was used to identify the organization of fibrillar components of the *Ossa cordis* bone matrix, as well as the fibrous tissue connected to the *Ossa cordis*. The *Ossa cordis dextrum* comprised trabecular bone tissue surrounded by fibrous tissue. Interconnecting vascular spaces were separated between the *Ossa cordis* bony trabeculae and connected to the marrow cavity (Figs. 16a–16c). The trabecular bone tissue was lamellar bone, organized into osteonal patterning, with concentric bone lamellae surrounding a central (osteonic or Haversian) canal. Interstitial lamellae were located between

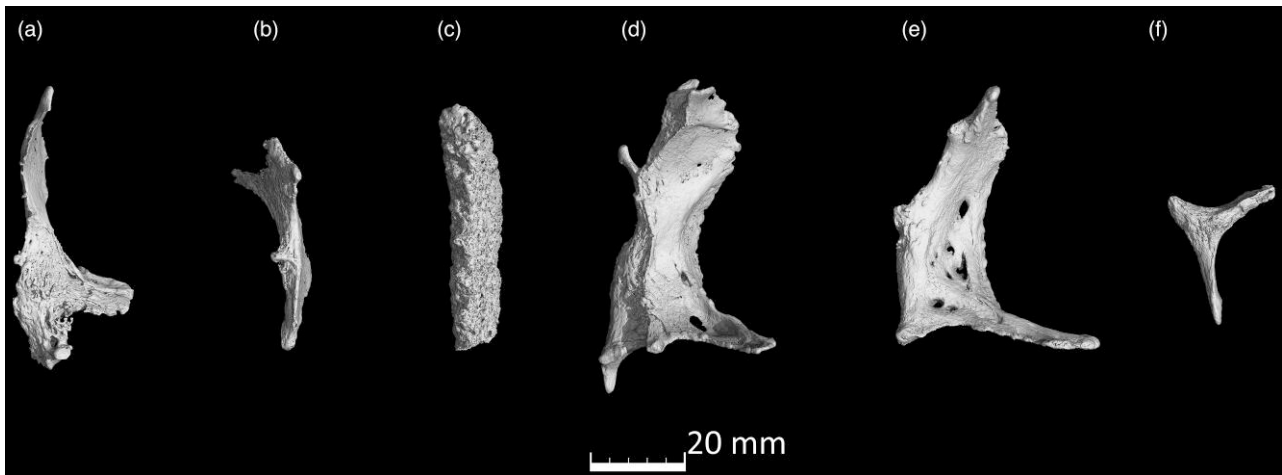


**Fig. 2.** microCT scans of *Ossa cordis dextrum*. (a–f) Six *Ossa cordis dextrum* exhibiting the differing bone shapes observed in different individuals.

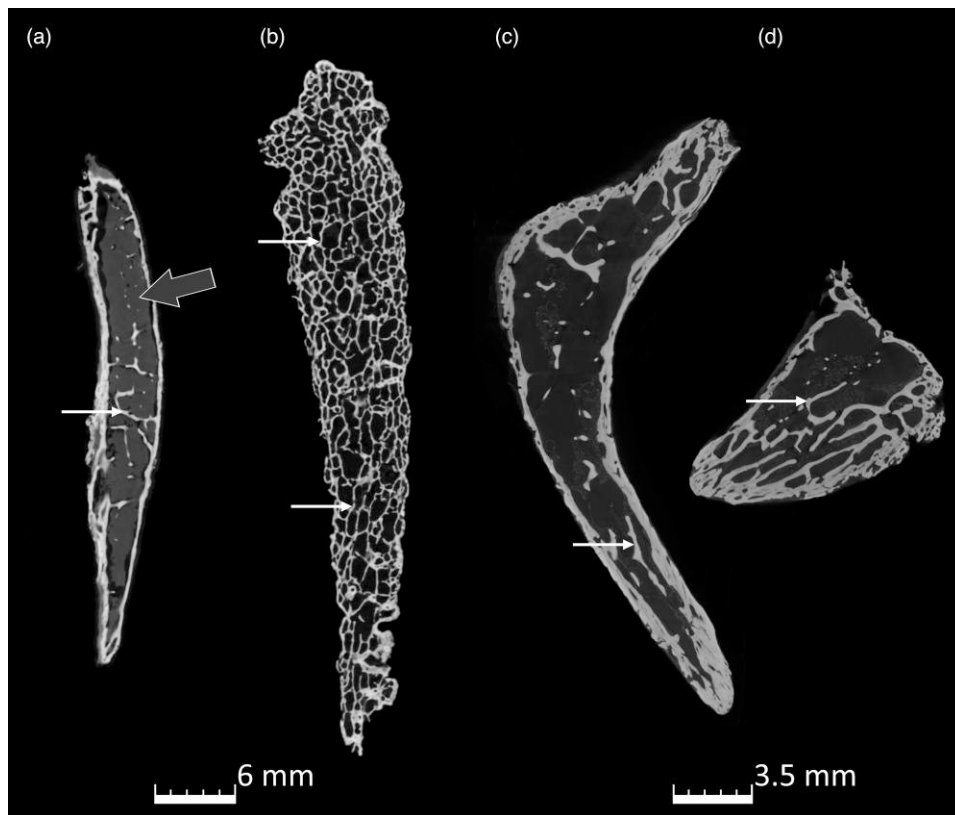


**Fig. 3.** microCT scans of the internal trabeculation of *Ossa cordis dextrum*. (a–d) Three different *Ossa cordis dextrum* indicating trabeculations (small white arrow) and bone marrow (gray arrow). (c,d) The same sample with sections extracted from the middle and cranial parts of the *Ossa cordis*.

adjacent osteons (Figs. 16d, 16e). The *Ossa cordis* were surrounded by the outer layer of the periosteum, which consisted of fibrovascular tissue. Sharpey's fibers, also called perforating fibers, consisted of bundles of periosteal collagen fibers that connected the periosteum to the bone, traversing through the bone matrix (Fig. 16f). Adjacent osteons were oriented perpendicular to each other (Fig. 16g). The peripheral layers of bone were randomly organized, forming woven bone, while the deeper bone tissue was uniformly organized, forming lamellar bone (Fig. 16h).

### *Histological Characterization of Ossa Cordis Using Crossman's Trichrome*

Crossman's trichrome stain was used to detect the organization of fibrous components in the *Ossa cordis dextrum* and the surrounding fibrous elements. As observed with the other stains, the *Ossa cordis* comprised trabecular bone tissue surrounded by fibrous tissue (Figs. 17a, 17b). This stain also confirmed that the bone trabeculae consisted of lamellar bone, organized into osteonal lamellae, and peripheral woven bone that had randomly organized bone fibrous



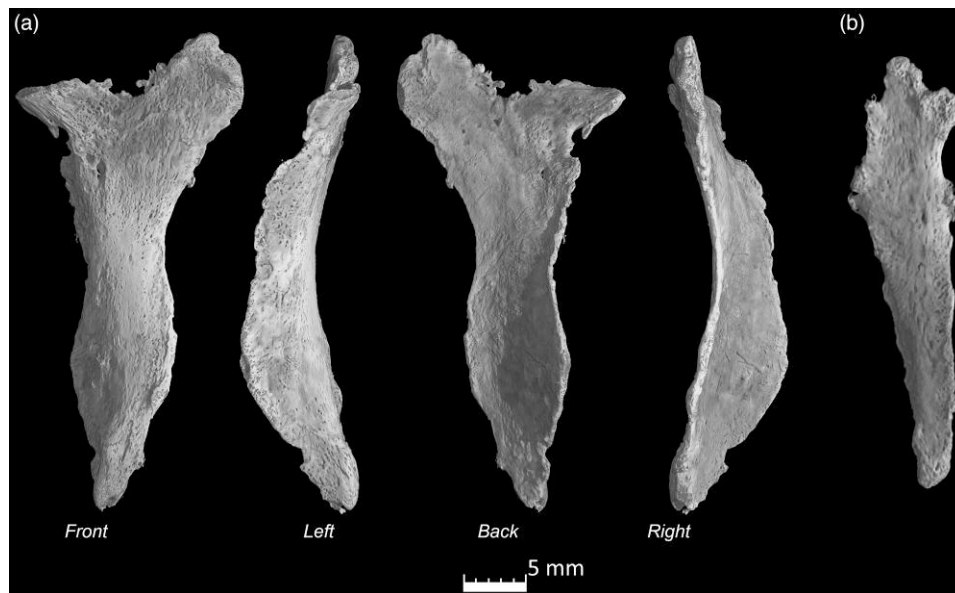


**Fig. 4.** microCT scans of the *Ossa cordis sinistrum*. (a) *Ossa cordis sinistrum* from four angles high resolution and (b) lower resolution of another *Ossa cordis sinistrum*.

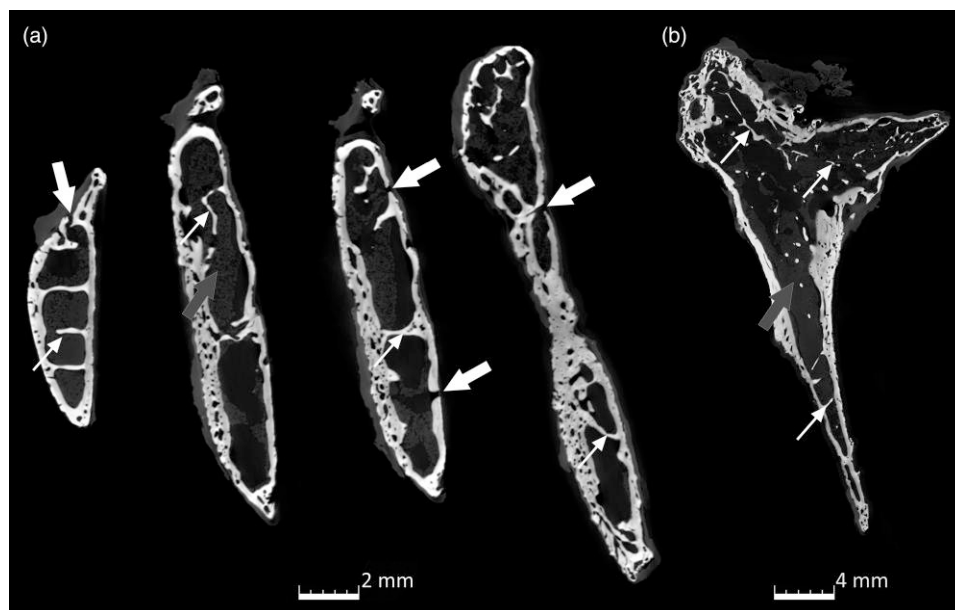


**Fig. 5.** microCT scans of the internal trabeculation of *Ossa cordis sinistrum*. (a) XY axis and (b) ZY axis indicating trabeculations (small white arrow), bone marrow (gray arrow), and holes in the *Ossa cordis sinistrum* bone.

components. The marrow cavity contained hematopoietic tissue and adipocyte cells (Figs. 17c, 17d). The trabecular bone had deeply stained bone lamellae and lightly stained interstitial lamellae (Fig. 17e), and the *Ossa cordis* had a thick trabecular bony plate and intercommunicating vascular spaces (Fig. 17f).

#### *Histological Characterization of Ossa Cordis Dextrum Using Alcian Blue Van Gieson*

Alcian blue Van Gieson detected the orientation of fibrous elements within the *Ossa cordis dextrum* as well as carbohydrate-rich components. The *Ossa cordis* consisted of

trabecular bone tissue located in the heart (Fig. 18a). The periosteum appeared as a fibrovascular tissue covering the bone trabeculae (Fig. 18b). The marrow cavity contained hematopoietic tissue and fat cells (Figs. 18c, 18d), as observed using the other stains. Sharpey's fibers (perforating fibers), consisting of bundles of periosteal collagen fibers, penetrated the bone matrix and connected the periosteum and the bone. The outer (peripheral) layers of the trabecular bone were formed from woven bone, with irregularly organized collagen fibers. Fibrocartilage connected the bone tissue and the cardiomyocytes (Figs. 18e, 18f). The trabecular bone also had interconnecting vascular spaces around which osteoblasts had formed osteons. Interstitial lamellae were located between



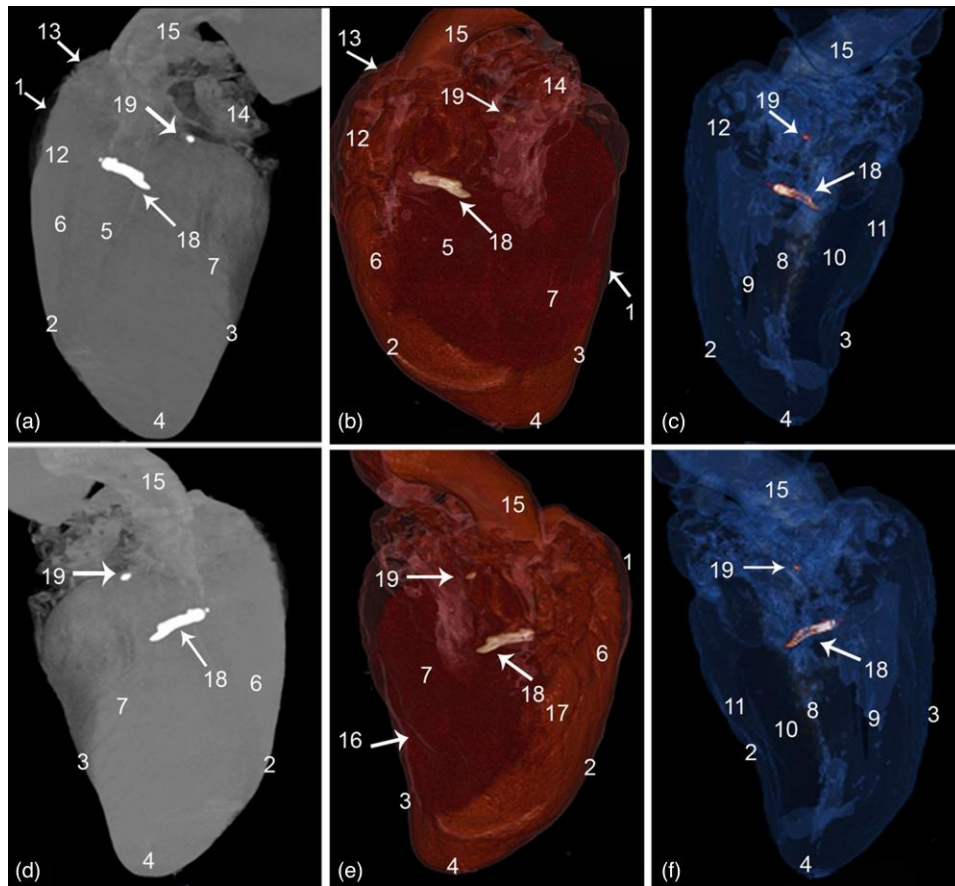


**Fig. 6.** CT 3D rendered volume of the cattle heart showing the *Ossa cordis dextrum* and *sinistram*. (a–c) Left view and (d–f) right view. (a,d) Ghost (black and white), (b,e) color render, and (c,f) blue angiography without contrast media. 1. Pericardium cavity, 2. Cranial border, 3. Caudal border, 4. Apex, 5. Left longitudinal interventricular groove (sulcus interventricularis paraconalis), 6. Right ventricle, 7. Left ventricle, 8. Interventricular septum, 9. Right ventricular cavity, 10. Left ventricular cavity, 11. Ventricular wall, 12. Conus arteriosus, 13. Right auricle, 14. Left auricle, 15. Aorta, 16. Right longitudinal interventricular (sulcus interventricularis subsinuosus), 17. Intermediate longitudinal groove, 18. *Ossa cordis dextrum*, and 19. *Ossa cordis sinistram*.

adjacent osteons, and the interstitial lamellae were also associated with a carbohydrate-rich bone matrix. The periosteum covered the *Ossa cordis* and osteoblasts were visible covering the trabecular bone surfaces, while osteocytes were embedded inside lacunae within the bone (Figs. 19a, 19b, 19d, 19e, 19g). The *Ossa cordis* also had osteons in differing orientations, while other collagen lamellae were perpendicular to the collagen lamellae of the adjacent osteon, and interstitial lamellae were associated with carbohydrate-rich bone matrix (Figs. 19c, 19f).

#### *Histological Characterization of the Ossa Cordis Sinistram Using Crossman's Trichrome, Alcian Blue Van Gieson, and Sirius Red*

The *Ossa cordis sinistram* (where present) were located in the initial portion of the ascending aorta. Their histological structures were very similar to those observed in the *Ossa cordis dextrum* (shown in detail in Figs. 13–19). They consisted of trabecular bone, covered externally by the periosteum, and surrounded by fibrous tissue (Figs. 20a, 20b, 20e). The trabecular bone contained typical osteons, structurally comprised concentrically organized bone lamellae surrounding vascular channels. The peripheral parts of the *Ossa cordis sinistram* were woven bone, which disorganized fibrous components (Figs. 20c, 20d, 20f, 20g). Sharpey's perforating fibers

extended from the periosteal collagen fibers and created a link between the periosteum and the bone (Fig. 20h).

#### Discussion

The *Ossa cordis* were located on the right side of the heart near the interventricular and interatrial septa, beneath, and extending into, the right atrioventricular ring. The *Ossa cordis dextrum* was just below the base of the aorta, and the caudal aspect of the bone extended toward the coronary sinus, while the *Ossa cordis sinistram* inserted into the left atrioventricular. Our present study reflected previous findings (James, 1965; Pour, 2004).

The prevalence of the *Ossa cordis* was also investigated in the present study. In cattle (*B. taurus*), it is known that each individual may have one or two *Ossa cordis*, with the *dextrum* reported in 100% of “beef,” Holstein and Iranian breed adults (James, 1965; Habermehl & Schmack, 1986; Pour, 2004). The present study also showed an *Ossa cordis* prevalence of 100% in both the Egyptian Baladi cattle and Holstein-Friesian cattle (Table 2). The *Ossa cordis sinistram* was previously found in 37.5% of beef hearts ( $n = 3$  from 8) (James, 1965) and 80% of Holstein breeds ( $n = 32$  from 40) and 20% of native Iranian cattle ( $n = 8$  from 40) (Pour, 2004). The present study showed 80% in the Egyptian Baladi cattle breed and 57% in the Holsteins. The *Ossa cordis*

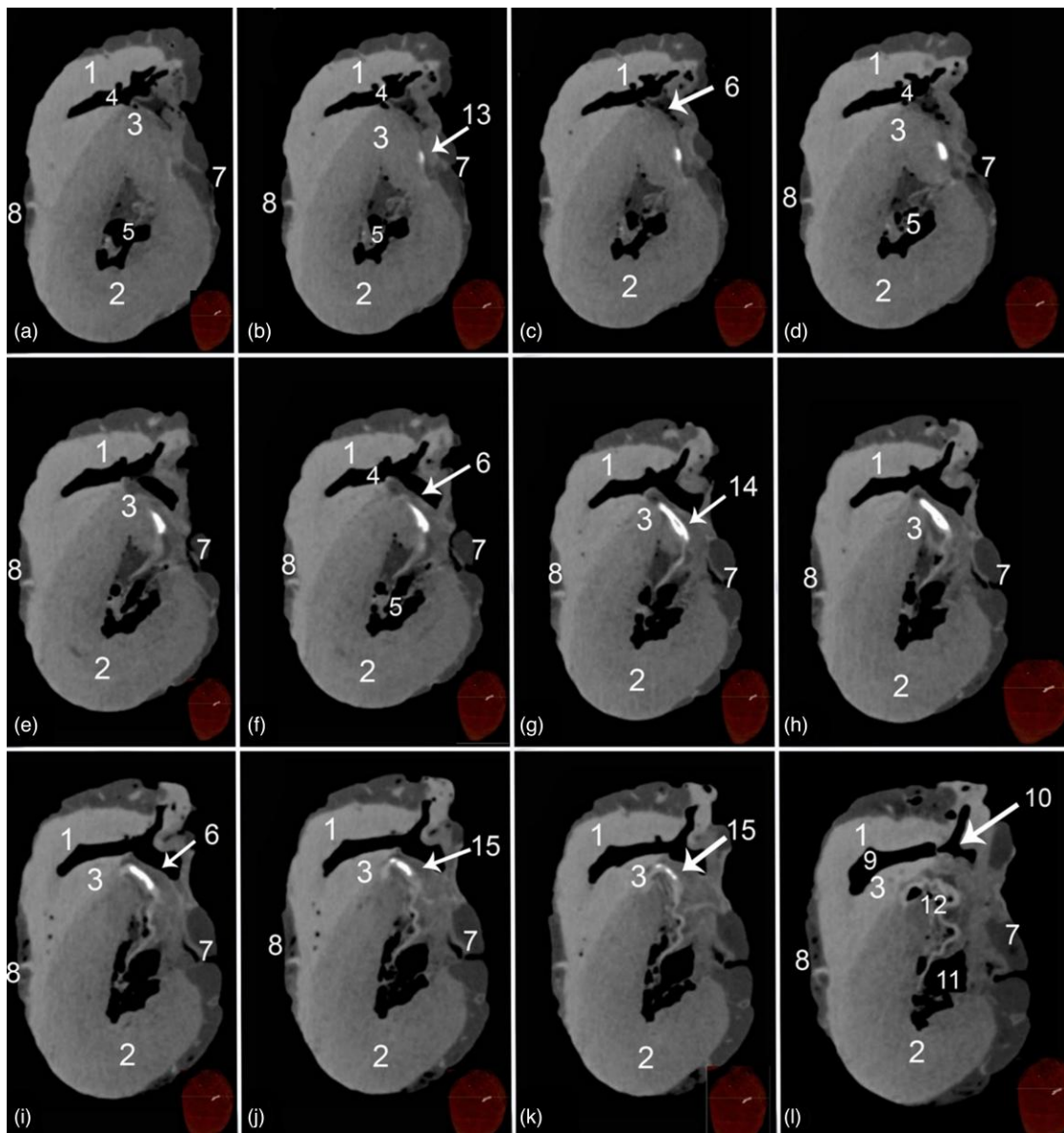


**Fig. 7.** Transverse soft tissue window CT scans at the proximal parts of the ventricular mass of a heart containing *Ossa cordis dextrum*. 1. Right ventricular wall, 2. Left ventricular wall, 3. Interventricular septum, 4. Left ventricular cavity, 5. Right ventricular cavity, 6. Septal wall near to the right interventricular orifice, 7. Right longitudinal interventricular (sulcus interventricularis subsinuosus), 8. Left longitudinal interventricular groove (sulcus interventricularis paraconlais), 9. Conus arteriosus, 10. Tricuspid valve, 11. Bicuspid valve, 12. Aorta, 13. Cranial cross section of *Ossa cordis dextrum* (note its small oval shape), 14. Middle cross section of *Ossa cordis dextrum* (oval to rectangular shape), and 15. Caudal cross section of *Ossa cordis dextrum* (oval through to circular shape).

*sinistrum* is therefore more variable possibly in differing breeds but also possibly in differing ages; it is worth noting that not all of the previous studies mentioned specific breeds or ages, and therefore, it is difficult to draw conclusions, but it may be worth future studies stating these factors.

*Ossa cordis* morphology and structures were also investigated via gross anatomical investigations including measurements, microCT, and electron microscopy. The shapes of each *Ossa cordis* (both *dextrum* and *sinistrum*), in both the previously published literature (Barasa & Gobetto, 1957; James, 1965; Pour, 2004) and within the present study differed significantly between individual animals. Figures 1 to 5 show the breadth of shape, generally though the caudal end was wider, and the cranial end was narrower, but this was not the case for every *Ossa cordis*. The literature has shown

that shape also varies between species, with some, such as the chimpanzee expressing a more oval-shaped *Ossa cordis*, elongated in sheep and goats (Mohammadpour, 2007), very irregular shapes in the otter (Egerbacher et al., 2000), and very frequently the shape was not discussed or shown; however, the present paper was able to show shape given the gross anatomical dissections and microCT undertaken.

*Ossa cordis* measurements also vary greatly between species; the largest published length was in an elephant at 80 mm (Endo et al., 2005), followed by the buffalo (*dextrum*) at 55 mm (David, 1937), cattle (*dextrum*) at 51 mm (James, 1965), to the smallest reported *Ossa cordis* in chimpanzees averaging 6.1 mm and otters ranging from 1.5 to 5 mm (Egerbacher et al., 2000; Moittie et al., 2020; Best et al., 2022). Previous cattle publications (summarized alongside

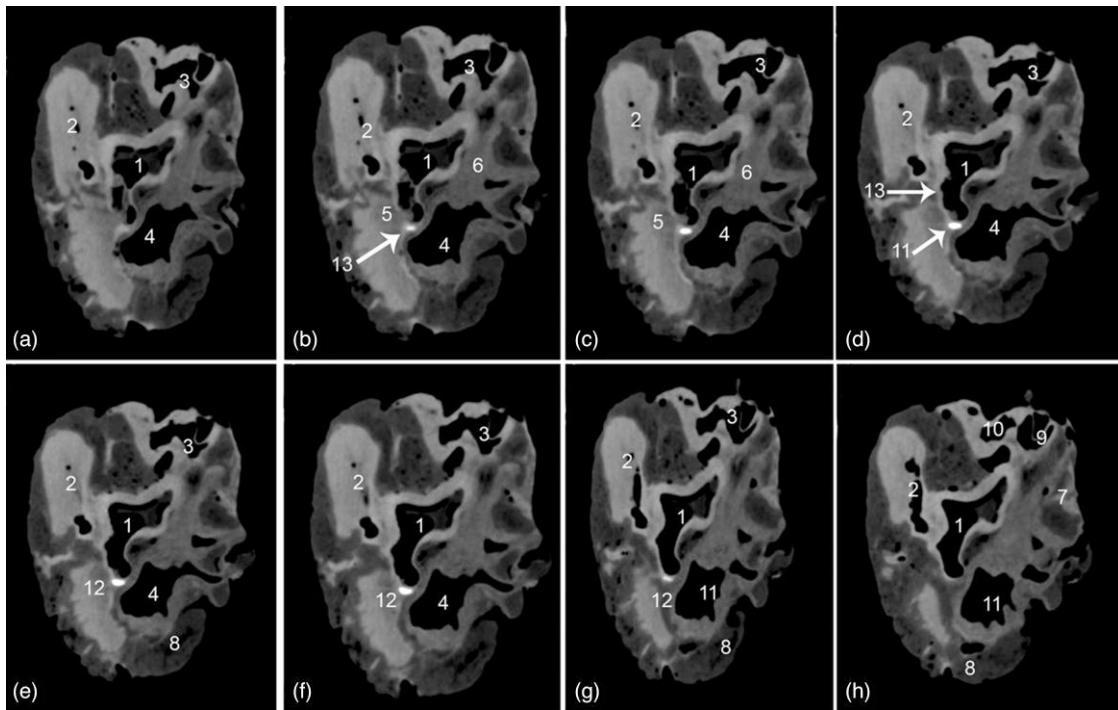


**Fig. 8.** Transverse soft tissue window computed tomography scans within the base of the heart displaying the *Ossa cordis sinistram*. (a–h) Scans taken at different points throughout the heart. 1. Aortic orifice (valve), 2. Pulmonary trunk valve, 3. Right atrioventricular orifice, 4. Left atrioventricular opening, 5. Left trigone, 6. Right trigone, 7. Right auricle, 8. Left auricle, 9. Caudal vena cava, 10. Cranial vena cava, 11. Pulmonary veins, 12. *Ossa cordis sinistram*, and 13. Aortic wall.

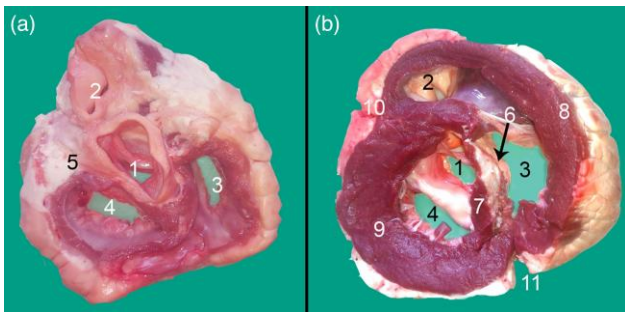


**Fig. 9.** Transverse cross section at the base of the heart displaying the *Ossa cordis dextrum*. (a) Dorsal view and (b) Ventral view. 1. Aortic orifice (valve), 2. Pulmonary trunk valve, 3. Right atrioventricular orifice, 4. Left atrioventricular opening, 5. Left trigone, 6. *Ossa cordis dextrum*, 7. Interventricular septum, 8. Right ventricular wall, 9. Left ventricular wall, 10. Left longitudinal interventricular groove (sulcus interventricularis paraconalis), and 11. Right longitudinal interventricular (sulcus interventricularis subsinuusus).

our present results in Table 2) have only reported on the length and width of the *Ossa cordis*, which has ranged from 40.85 to 51.00 mm long (average calculated across studies 40.92 mm) and 4.00–7.49 mm at the least wide part to 8.40–18.36 mm at the widest part of the *Ossa cordis dextrum* (James, 1965; Pour, 2004; Best et al., 2022). In the *Ossa cordis sinistram*, the published lengths in cattle have ranged between 17.35 and 19.95 mm (average 18.43 mm), with a width of 7.28–11.60 mm (average 9.54 mm) (James, 1965; Pour, 2004). It is important to note that the previous studies did not always state whether these were the widths at the greatest, the least, or an average of several widths, importantly given the

variation of widths observed across the bones. The present study measured the greatest length, and for width and depth measured the thinnest and thickest parts of each bone. It is also worth noting that the Egyptian Baladi *Ossa cordis dextrum* and *sinistram* in the present study were smaller than the Holstein-Friesian *Ossa cordis*; therefore, it is likely that breed, or breed size, may also impact *Ossa cordis* size. The Holstein-Friesian steer presently weighs 545–635 kg on average, whereas the Egyptian Baladi is lighter at around 350–400 kg (Morsy et al., 1984; Boersema et al., 2010). It is also essential to note that the previous studies were many decades ago and cattle size in general has changed over time, and also, breeds, ages, and sexes were also not always mentioned or differentiated in the previously published works. The Egyptian Baladi cattle in the present study showed similar *Ossa cordis dextrum* and *sinistram* measurements to the previous studies, whereas the Holstein-Friesian were generally larger, but it is important to note the caveats when comparing directly between the differing sets of measurements previously published. A final point regarding *Ossa cordis* size was that *dextrum* was larger in both of our cattle breeds than the *sinistram*, in line with previous observations in other cattle and in other species (James, 1965; Pour, 2004; Best et al., 2022).

Cartilaginous material was present within this study, and this is the first time the elemental composition has been shown for *Ossa cordis* and the surface cartilage in any species; however, further studies are required to understand the exact composition of these tissues. The cartilaginous tissue, both within and surrounding the *Ossa cordis dextrum* and *sinistram*, is notably variable in relation to identification or presence in previous publications. One previous study suggested that the two *Ossa cordis* were always connected by cartilage (James, 1965);



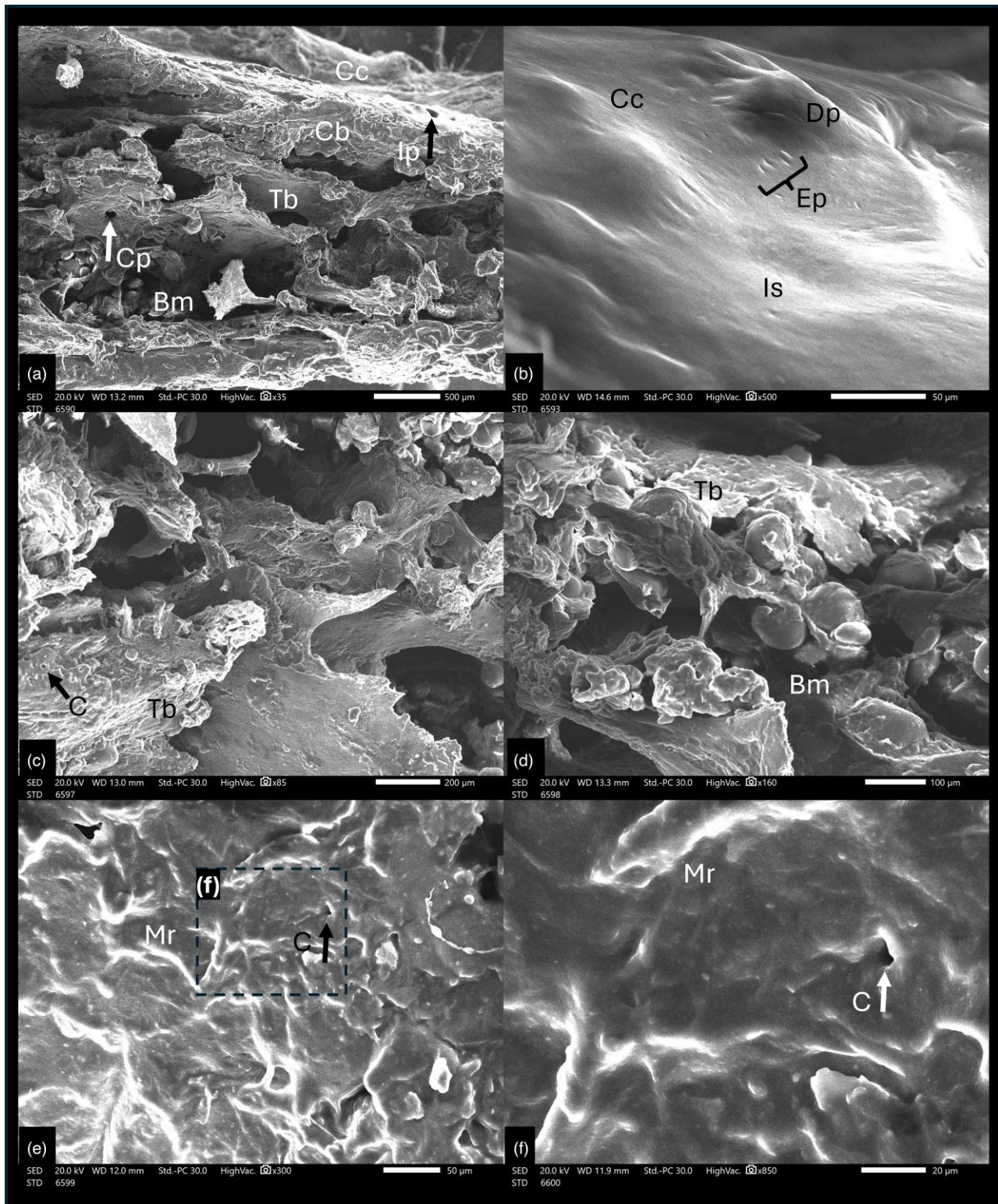


**Fig. 10.** Scanning electron microscope cross section of cattle *Ossa cordis dextrum*. (a) Cross section through *Ossa cordis* and cartilage layer and (b) Cartilage surrounding the *Ossa cordis*. (c–f) Inner structures of *Ossa cordis*. Bm, bone marrow space/medullary cavity; C, canaliculi pore; Cb, cortical bone; Cc, cartilage covering the *Ossa cordis*; Cp, circular large pores on the flat trabecular bone; Dp, dome-shaped projections of cartilage; Ep, elliptical shaped pores; Ip, irregular pores in the cortical bone on the external surface; Is, irregular external surface of the cartilage surrounding the *Ossa cordis*; Mr, Micro-ridges—forming in irregular/nonuniform directions; Tb, trabecular bone—flat and wide shaped.

however, in a more recent study, no cartilaginous connection was reported (Pour, 2004). A cartilaginous connection between the *Ossa cordis dextrum* and *sinistrum* (where both were observed) was not observed in this study; the bones

were covered in cartilage, but myocardium was observed around each structure with no interconnecting cartilage. It is possible that cartilage may or may not develop at different stages, such as when the *sinistrum*, for example, is developing,



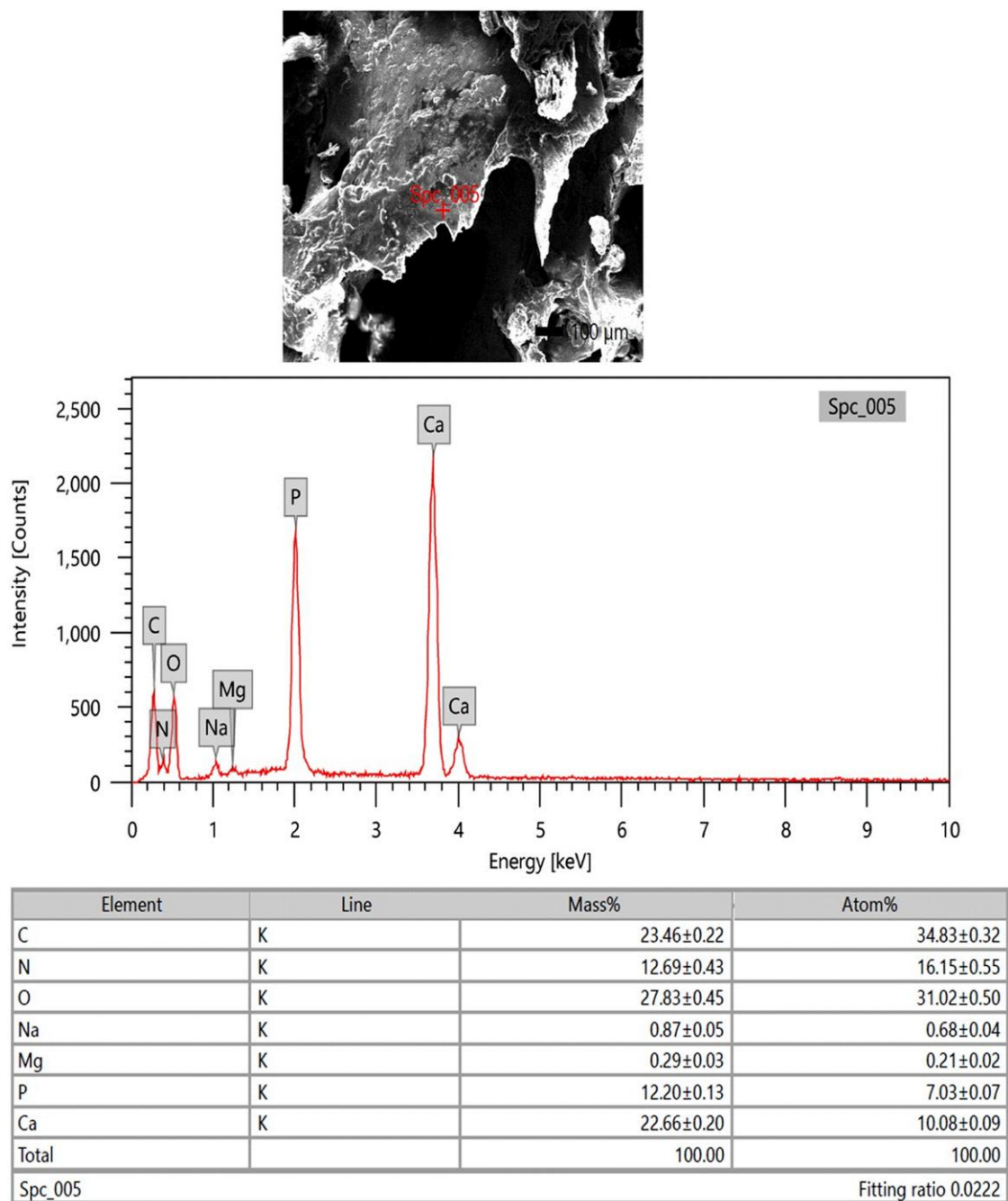


**Fig. 11.** SEM-EDX investigation of the *Ossa cordis dextrum* trabeculations. SEM-EDX image, graphical representation, and table of elements and their masses. The expressed elements were oxygen, carbon, calcium, nitrogen, phosphorus, sodium, and magnesium.

or indeed if both bones are relatively near to each other, but at the time point looked at in each individual, this was not observed. It has been hypothesized that the formation of *Ossa cordis* occurs via endochondral ossification rather than intramembranous ossification (Moittie et al., 2020; Best et al., 2022). We did not observe a *Cartilago cordis* (instead of an absent *Ossa cordis sinistrum*), which could have indicated potential *Ossa cordis* developmental processes if present, but cartilage was present in/surrounding each *Ossa cordis dextrum* and *sinistrum*. In buffaloes, it was noted that in a young animals (less than 30 days), cartilage was present but no *Ossa cordis*, whereas adults had an *Ossa cordis* in the same

anatomical location (Daghash & Farghali, 2017). The previously published literature does not always mention cartilage in association with *Ossa cordis*; however, the present research confirms that it is present in cattle; this alone cannot verify endochondral ossification, but it further supports the theory.

Histologically, the *Ossa cordis dextrum* and *sinistrum* bones were structurally similar to other types of trabecular (also known as cancellous or spongy) bone observed elsewhere in the body. The lamellae and osteons were present inside the trabeculae and a periosteum created an exterior layer of fibrovascular tissue encapsulating the osseous tissue. The periosteum was connected to the bone through penetrating fibers

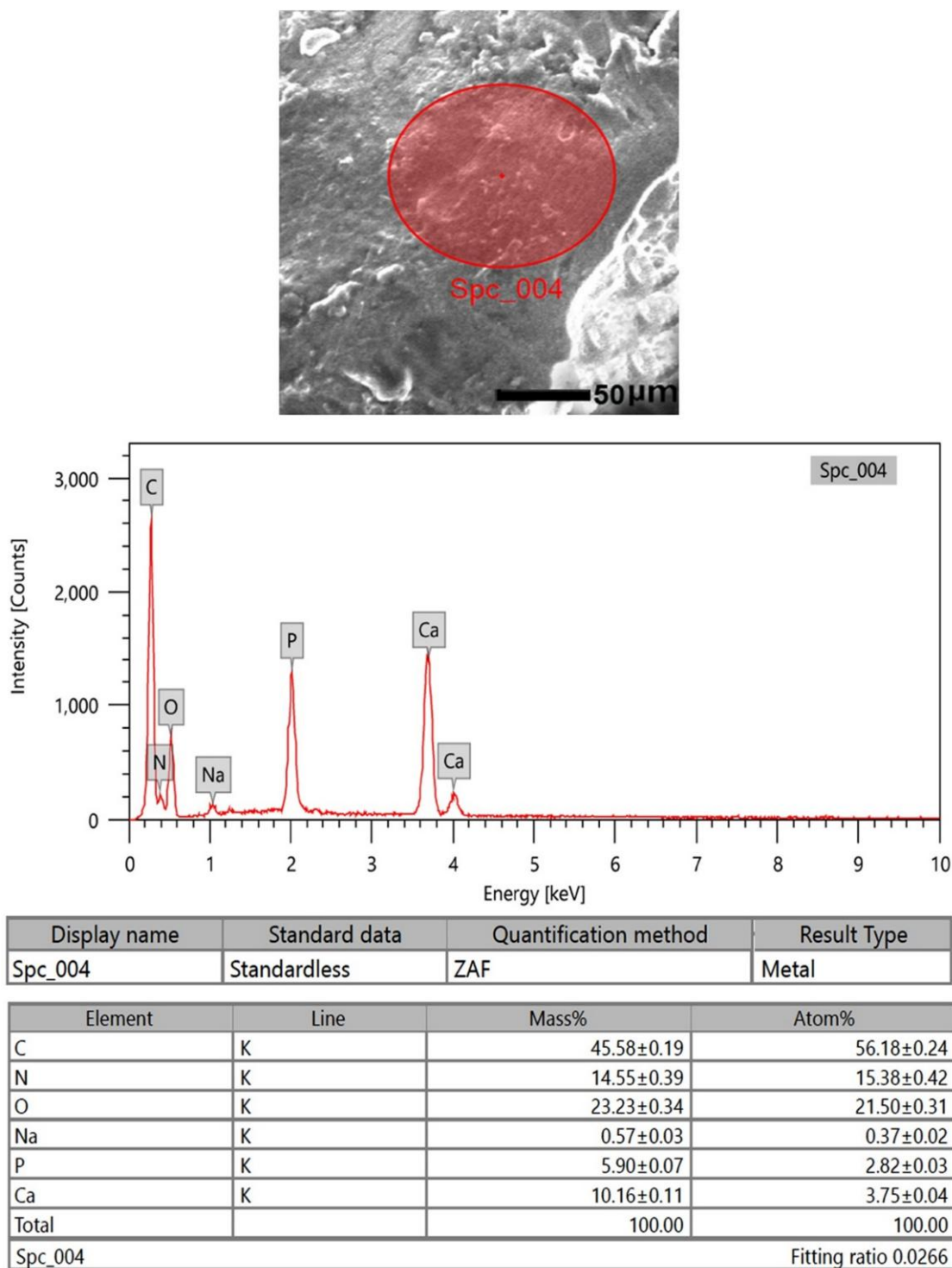


**Fig. 12.** SEM-EDX investigation of the *Ossa cordis dextrum* cartilaginous surface. SEM-EDX image, graphical representation, and table of elements and their masses. The expressed elements were carbon, oxygen, nitrogen, calcium, phosphorus, and sodium.

(likely Sharpey's fibers), bundles of periosteal collagen fibers. Certain fiber-detecting stains, such as Van Gieson and Sirius Red, have a mild staining affinity for interstitial lamellae, and this was observed in our histological examinations. Deterioration of the interstitial lamellae fibrous components may be the cause of this mild staining in comparison with the more intense staining observed elsewhere. Bone tissue is often shed and replaced by new bone lamellae, and interstitial

lamellae are often remnants of previous Haversian systems including the circumferential lamellae (Standring, 2016). As interstitial lamellae were observed between osteons in the present study, active growth and/or remodeling may be present within the *Ossa cordis*. In addition, we discovered a matrix rich in carbohydrates that was linked to the interstitial lamellae. Large numbers of glycosaminoglycans are generally found in the extracellular matrix. Rühland et al. (2007) found that



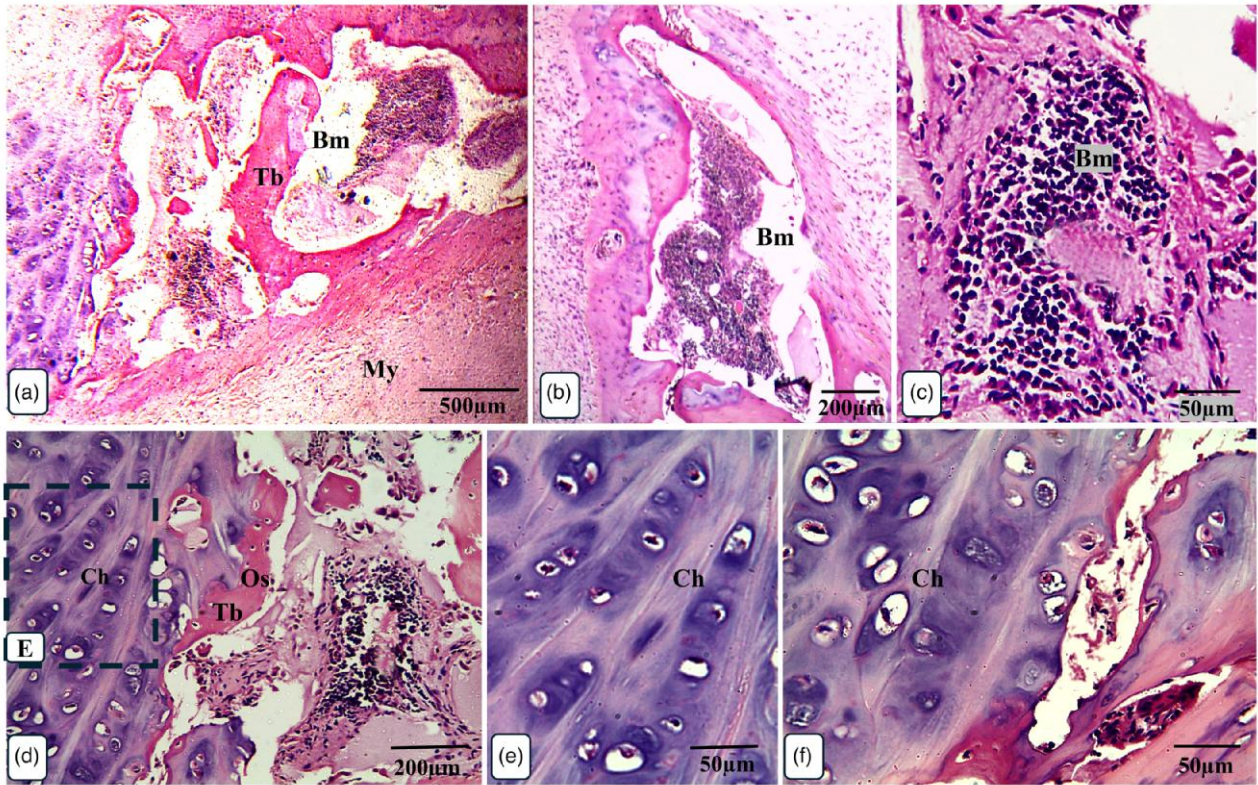


**Fig. 13.** Overview of *Ossa cordis dextrum* histology using H&E staining. Note the chondrocytes surrounding the cortical bone and trabeculations. Bm, bone marrow space/medullary cavity; Ch, chondrocytes; My, myocardium; Os, osteocytes; Tb, trabeculation.

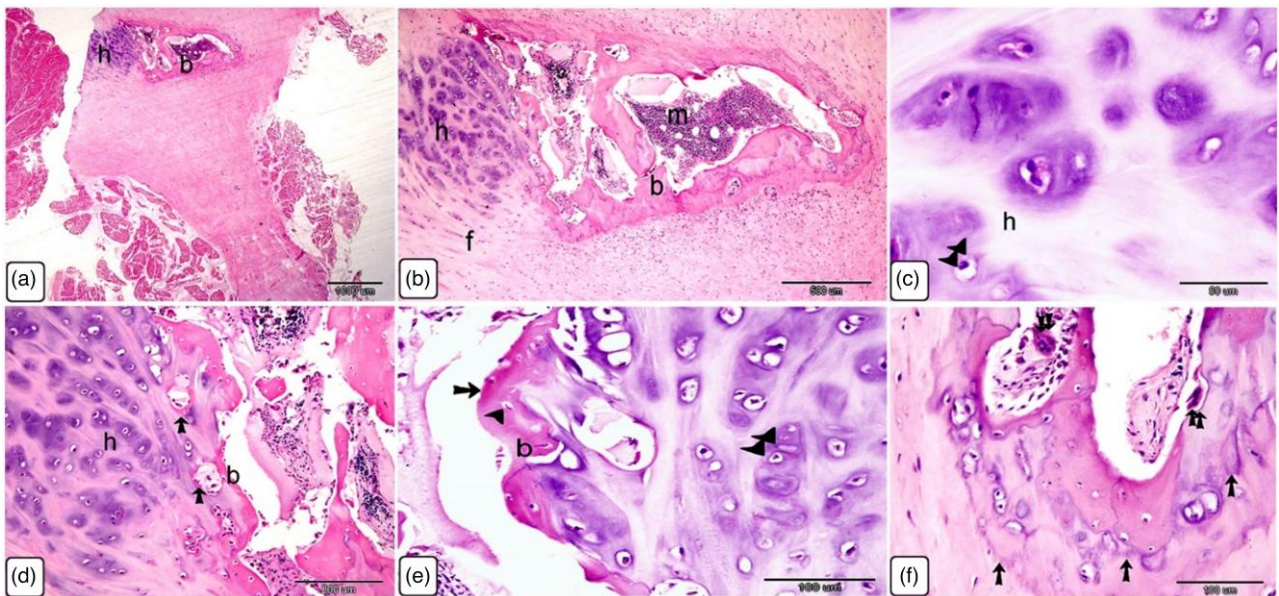


**Fig. 14.** Histological characterization of *Ossa cordis dextrum* using H&E. (a,b) The *Ossa cordis dextrum* consisted of trabecular bone tissue. Hyaline cartilage covered the surface of the bones. Hyaline cartilage (h) and the outer fibrous tissue were joined by fibrocartilage (f). (c-e): Chondrocytes (double arrowheads) were found in the hyaline cartilage (h) and were surrounded by cartilage matrix. Intracartilaginous ossification (arrow) was observed adjacent to bone growth, which was located inside the cartilage gap following chondrocyte death. Growth of bone tissue (arrow) was seen adjacent to the hyaline cartilage in e. Note that osteoclasts (double arrows) had many nuclei and an acidophilic cytoplasm. (f) Take note of the osteocytes (arrowheads) and chondrocytes (double arrowheads).

glycosaminoglycans are involved in the process of collagen fibrillogenesis. In addition, glycosaminoglycans, such as decorin and biglycan, are crucial components in the formation of

Type I collagen in bone tissue (Svensson et al., 1995); therefore, it was noteworthy to see these features in both the *Ossa cordis dextrum* and *sinistrum*. Another interesting



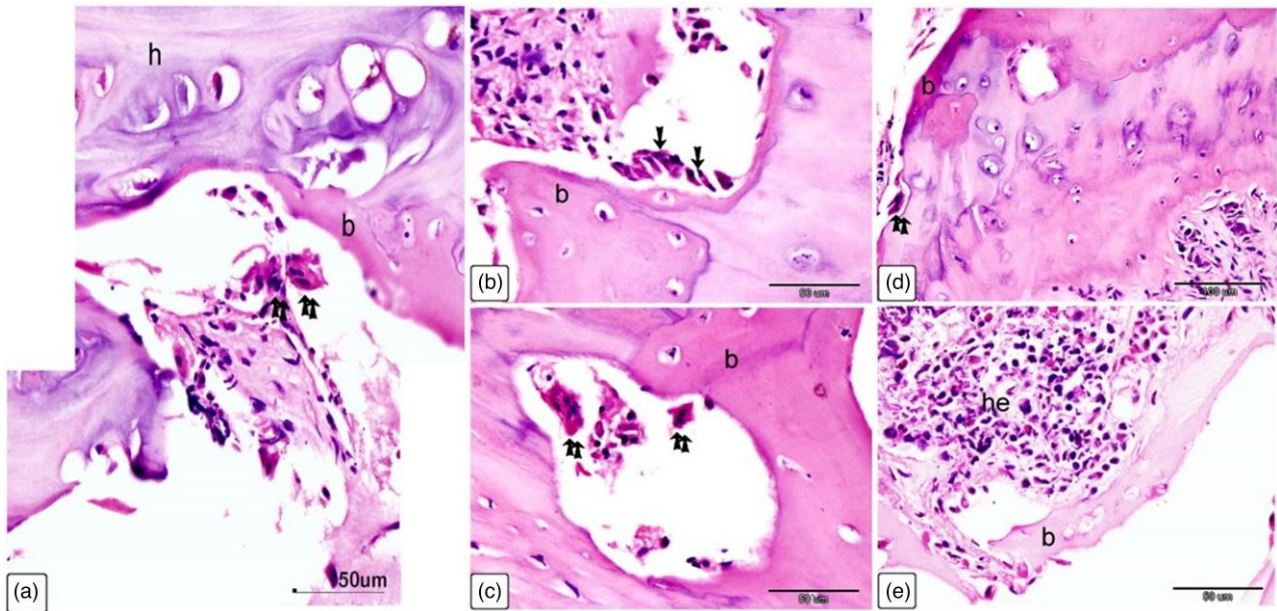


**Fig. 15.** Cellular characterization within *Ossa cordis dextrum* using H&E. (a) The *Ossa cordis dextrum* consisted of trabecular bone tissue (b), with hyaline cartilage (h) and osteoclasts (double arrows). (b) Osteoblasts (arrows) were present on the surface of bone trabeculae (b). (c) Osteoclasts (double arrows) were present within the Howship's lacunae and osteoprogenitor cells were present in the periosteum. (d) Osteoclasts (double arrows) were also observed in the bone marrow space. (e) Hematopoietic filled the holes within the bone marrow located between the trabeculae bone (b).

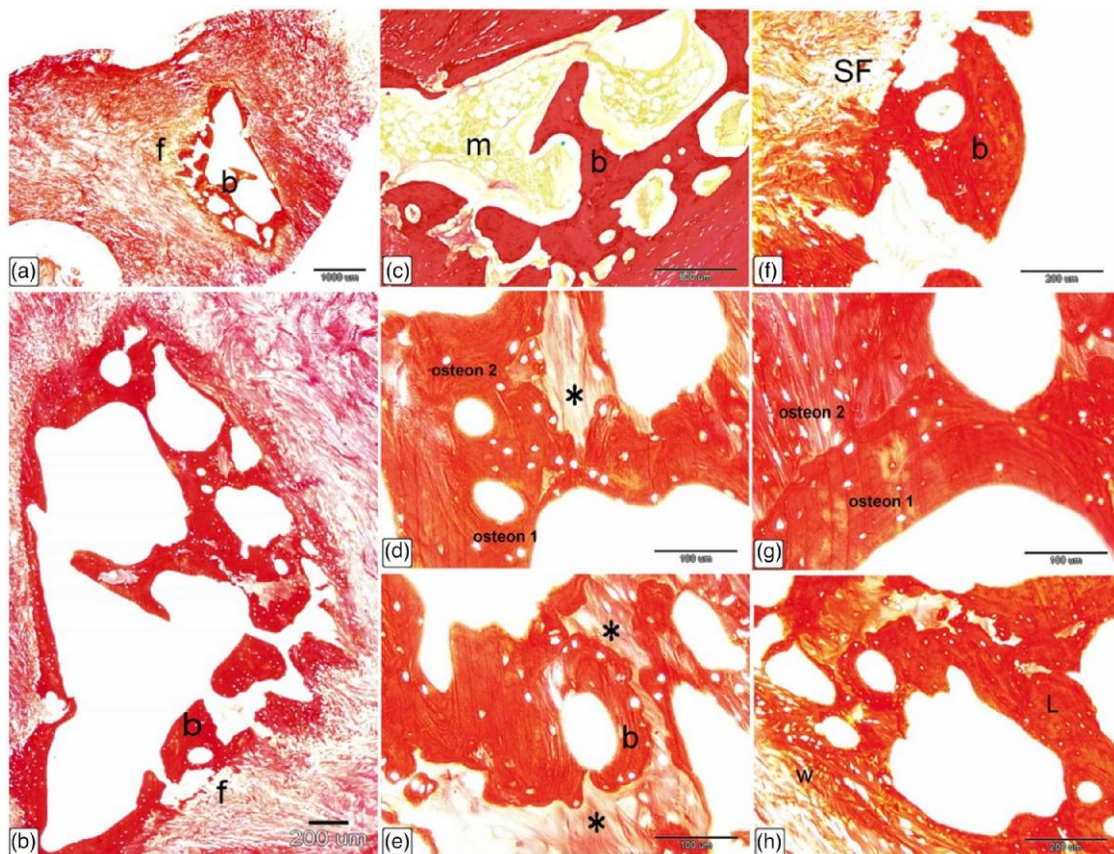


**Fig. 16.** Histological characterization of *Ossa cordis dextrum* using Sirius Red stain. (a–c) The *Ossa cordis dextrum* consisted of trabecular bone tissue (b) with fibrous tissue (f) surrounding it and bone marrow (m). (d,e) The trabecular bone tissue showed lamellar bone with osteon structures. Note that the osteons labeled 1 and 2 consisted of bone lamellae and arranged in concentric circles surrounding an osteonic cavity. There were interstitial lamellae (asterisks) between osteons that are next to each other. (f) The top layer of the collagen fiber periosteum covered the *Ossa cordis*. Sharpey's fibers, which are made up of bundles of periosteal collagen fibers, connected the periosteum to the bone by going through the bone matrix. (g) Two osteons were adjacent to each other but not parallel to each other. (h) The outer layers of bone contained randomly arranged woven bone (w), while the inner layers had more mature, regularly arranged lamellar bone (L).



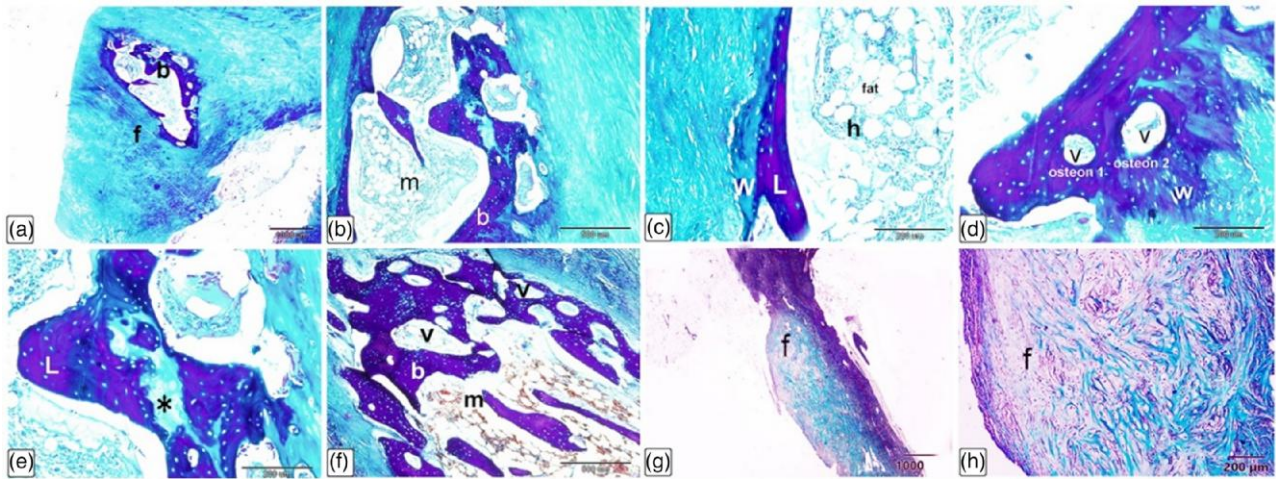


**Fig. 17.** Histological characterization of *Ossa cordis dextrum* using Crossman's trichrome. **(a,b)** The *Ossa cordis dextrum* consisted of trabecular bone (b) with fibrous tissue (f) around it and bone marrow (m). **(c)** The bone trabeculae contained both lamellar bone (L) and peripheral woven bone (W). Hematopoietic tissue (h) and adipocytes (fat) were present in the marrow cavity. **(d)** The osteons present in the trabecular bone also differentiated it from the woven bone (W). **(e)** The trabecular bone had bone lamellae that were strongly stained and interstitial lamellae that were lightly stained (asterisk). **(f)** The *Ossa cordis* had a thick trabecular bone wall and vascular spaces that connected to each other. **(g,h)** Fibrocartilage connected the *Ossa cordis* to the fibrous tissue (f) around it.

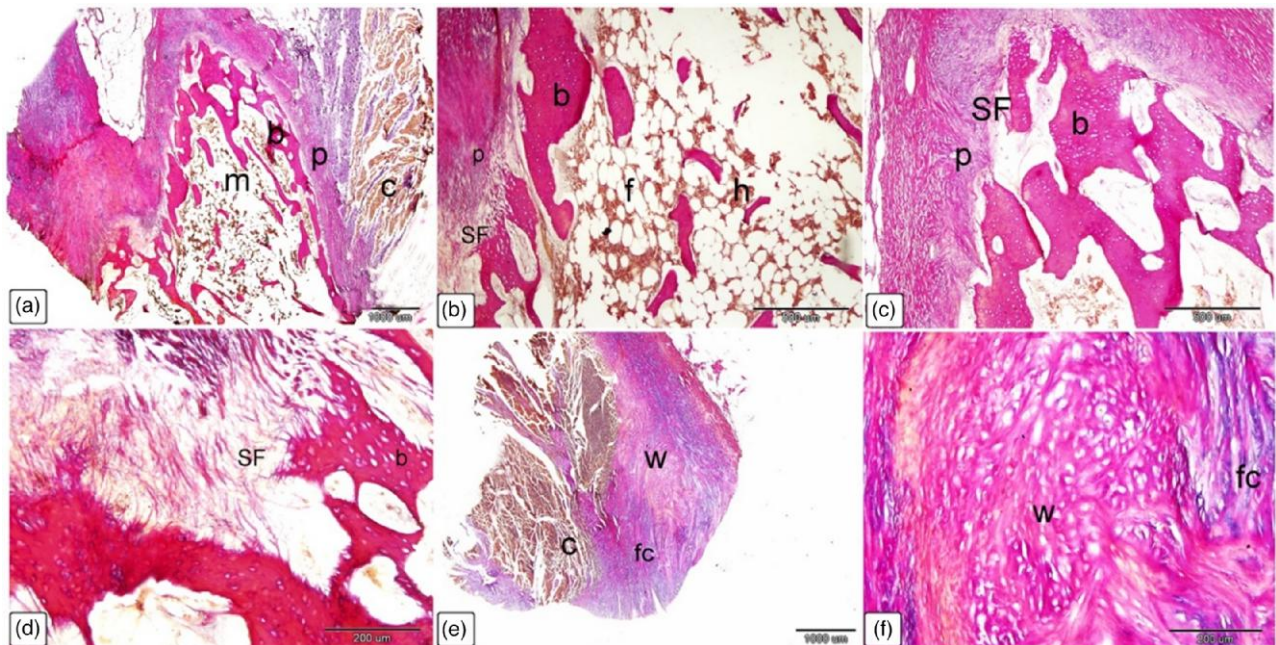


**Fig. 18.** Histological characterization of *Ossa cordis dextrum* using Alcian blue Van Gieson. **(a,b)** The trabecular bone (b) of the *Ossa cordis* contained cardiomyocytes (c), bone marrow spaces (m), and a vascularized soft tissue—the periosteum (p). **(c,d)** Hematopoietic tissue (h) and adipocytes [fat cells (f)] were present inside the bone marrow cavity. Sharpey's fibers, also known as perforating fibers, which are periosteal collagen fibers, went through the bone matrix and connected the periosteum to the bone. **(e,f)** The upper layers of trabecular bone consisted of woven bone, with disorganized collagen fibers. Fibrocartilage linked the cardiomyocytes (c) to the bone tissue.

bone structure observation in the present study was that neighboring osteons were generally perpendicular to one another, although not in all cases. As a result, the bone may be able to withstand endurance forces in a more tensile form. In addition to more mature lamellar bone, woven bone was also present in the *Ossa cordis*. Newly produced bone has a characteristic known as woven (or fibrous) bone, which contains haphazard collagen fiber arrangements. This new bone

growth may be linked to osteoblasts in the periosteum as these cells can produce new bone. In general (Moreira et al., 2000), lamellar bone eventually replaces woven bone, the more transient form, following bone maturation and/or repair. Renewal of the bone tissue within the *Ossa cordis dextrum* and *sinistrum* is thus indicated by the presence of low fibrous components of the interstitial lamellae, a matrix rich in carbohydrates, and the creation of new bone tissue.



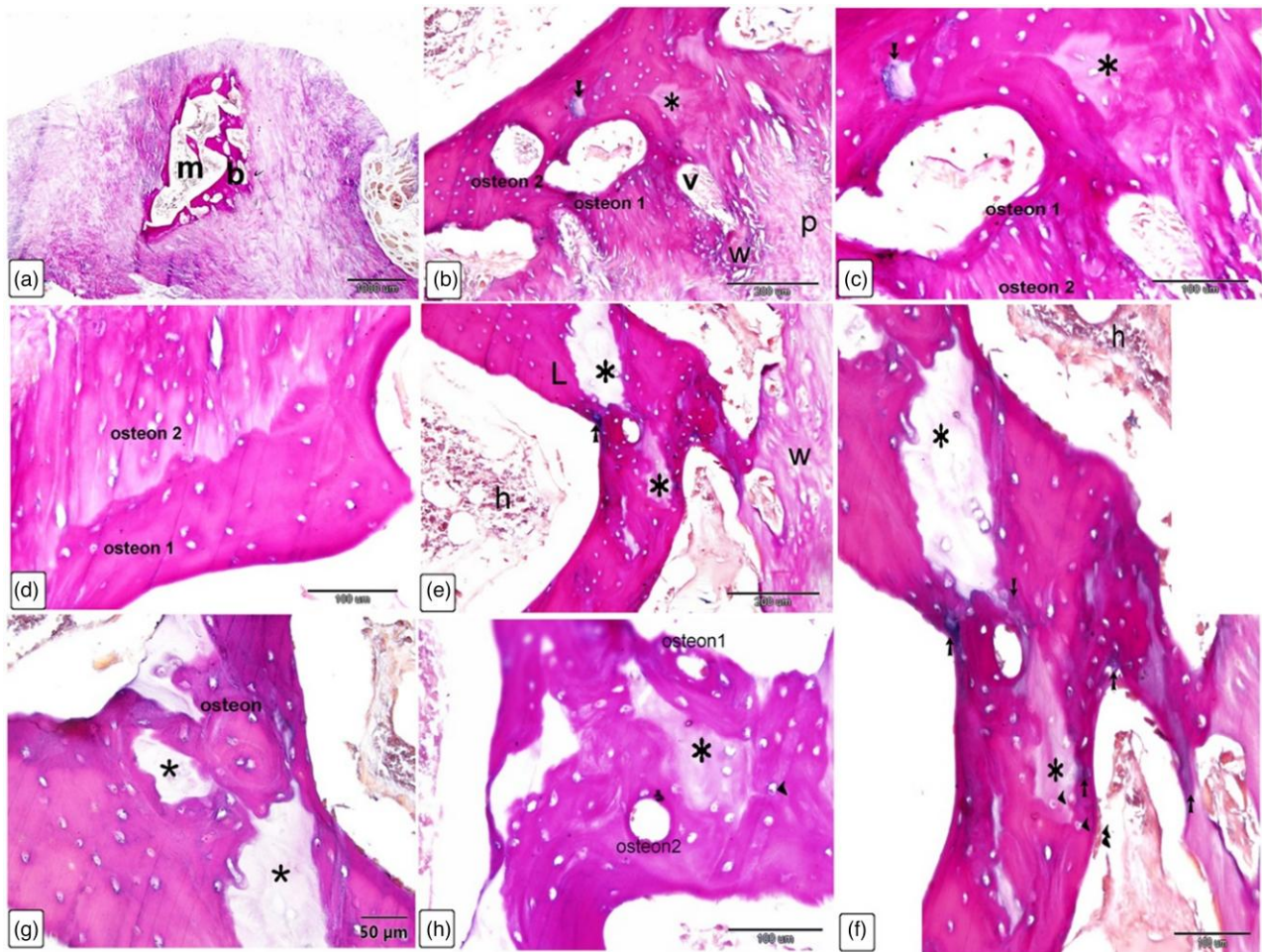


**Fig. 19.** Histological characterization of *Ossa cordis dextrum* using Alcian blue Van Gieson. (a) The trabecular bone tissue (b) surrounding the marrow space (m) was clearly visible using the Alcian blue Van Gieson stain. b–h: The trabecular bone (b) had venous spaces that connected to each other, and osteoblasts were present around these spaces with osteon structures present. There were interstitial lamellae (asterisks) between osteons that were next to each other, and notably the interstitial lamellae were associated to bone material that was high in carbohydrates (intense staining). The interstitial lamellae were connected to the bone matrix, which was high in carbohydrates (arrows). The collagen fibers in woven bone (w) were arranged in a random way. The periosteum (p) covered the *Ossa cordis*, and the trabecular bone surface was covered with osteoblasts (double arrowheads) and osteocytes (arrowheads) were visualized within lacunae. In cases (c) and (d), the osteons within the *Ossa cordis* bone tissues were oriented in different directions to each other, and the collagen lamellae were not parallel to the collagen lamellae of the neighboring osteon.

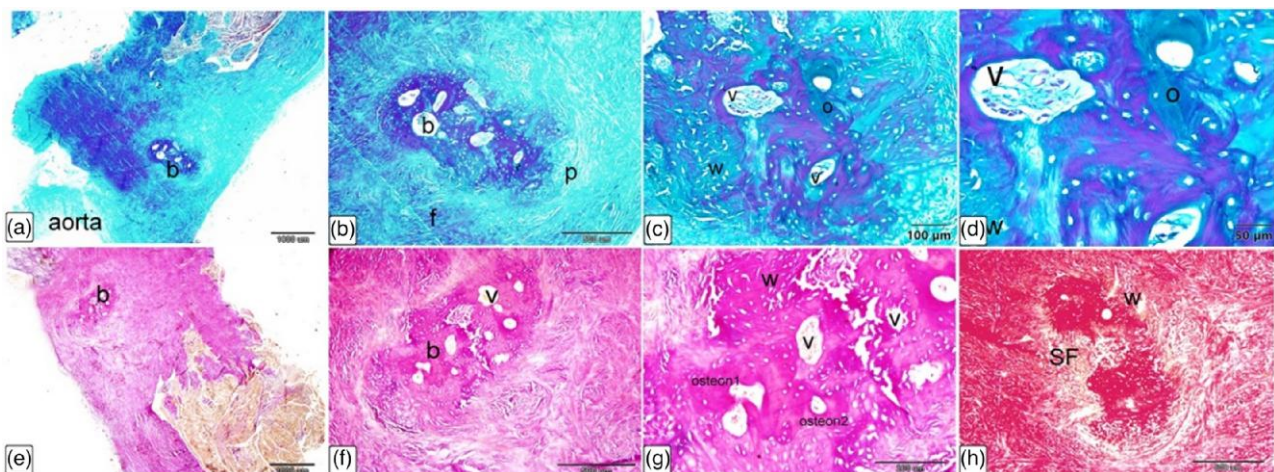


**Fig. 20.** Histological characterization of *Ossa cordis sinistrum* using Crossman's trichrome (a–d), Alcian blue Van Gieson (e–g), and Sirius Red (h). (a,b,e) The *Ossa cordis sinistrum* (where present) were located in the initial portion of the ascending aorta. They consisted of trabecular bone covered externally by a periosteum and were surrounded by fibrous tissue. (c,d,f,g) The *Ossa cordis sinistrum* trabecular bone had typical morphology osteons (o) with concentric organization of bone lamellae surrounding vascular channels (v). The peripheral parts of the bone tissue consisted of woven bone (w), which was distinguished from the lamellar bone due to the disorganized structure of the fibrous components. (h) Sharpey's perforating fibers (fibers) extended from the periosteal collagen fibers and linked the periosteum and the bone.

**Table 2.** Comparison of Published *Ossa Cordis* Measurements in Cattle.

Species, bone	Length (mm)	Width (mm)	Depth (mm)	Prevalence % (total <i>n</i> studied)	References
Buffalo, dextrum	52	13	—	93% (15)	(Daghash & Farghalii, 2017)
	40–55	20–30, 2–6 (base, apex)	—	83% (6)	
Buffalo, sinistrum	23	4	—	93% (15)	(Daghash & Farghalii, 2017)
	23–30	—	—	83% (6)	
Cattle, dextrum	40.85	7.49, 18.36	—	100% (40)	(David, 1937) <sup>a</sup> (Pour, 2004) (Pour, 2004) (James, 1965)
	30.92	5.25, 10.99	—	100% (40)	
	51.00	4.00, 8.40	—	100% (8)	
	$\bar{x} = 40.92$	$\bar{x} = 5.58, 12.58$ (cranial, caudal)	—	—	
Cattle, sinistrum	19.95	9.75	—	100% (40)	(Pour, 2004) (Pour, 2004) (James, 1965)
	17.35	7.28	—	100% (40)	
	18.00	11.60	—	37.5% (8)	
	$\bar{x} = 18.43$	$\bar{x} = 9.54$	—	—	
Present study					
Egyptian Baladi cattle, dextrum	43.68	12.59 <sup>b</sup>	3.67 <sup>b</sup>	100% (5)	Present study
Egyptian Baladi cattle, sinistrum	18.63	9.00 <sup>b</sup>	4.00 <sup>b</sup>	80% (4)	Present study
Holstein, dextrum	55.71	26.86 <sup>b</sup>	6.63 <sup>b</sup>	100% (7)	Present study
Holstein, sinistrum	31.25	16.50 <sup>b</sup>	4.21 <sup>b</sup>	57% (4)	Present study

<sup>a</sup>Measured from a scaled image (Best et al., 2022).

<sup>b</sup>Note thickest part measured in the present study, previous study did not state thinnest/thickest or type of measurement. Table was adapted from Best et al. (2022), with additional information added from the present study.

## Conclusions

This research has shown the macro and microscopic features of both the Egyptian Baladi cattle and Holstein-Friesians using scanning electron microscopy, X-ray microtomography, gross dissections and measurements, histology staining and microscopy, and energy dispersive X-ray analysis. This is the first investigation to show bone maturation or renewal in *Ossa cordis*, which highlights the potential for bone growth within these heterotopic bones. This research also exhibited the detailed gross and microscopic structures and components of the *Ossa cordis* and associated cartilaginous tissue, including trabecular bone, lamellae and osteons, a periosteum, collagen fibres, and glycosaminoglycans and carbohydrates. Cartilage was observed both within, and surrounding, the *Ossa cordis* and the elemental composition of the bone and cartilage was detected using dispersive X-ray analysis.

## Availability of Data and Materials

The data supporting this study's findings are available from the corresponding author upon reasonable request. Due to ethical constraints, the data are not publicly available.

## Supplementary Material

To view [supplementary material](https://doi.org/10.1093/mam/ozae046) for this article, please visit <https://doi.org/10.1093/mam/ozae046>.

## Acknowledgments

The authors would like to thank the SVMS anatomy technical team for some specimens.

## Financial Support

We thank Alexandria University and the School of Veterinary Medicine and Science, University of Nottingham for funding. The Hounsfield Facility received funding from the European Research Council (Future Roots Project), Biotechnology and Biological Sciences Research Council of the United Kingdom, and The Wolfson Foundation.

## Conflict of Interest

The authors declare that they have no competing interest.

## Ethical Standards

All experimental protocols were approved by the Institutional Animal Care and Use Committee (ALEXU-IACUC) of the Alexandria University (Approval No: AU/13/2023/02/01/212). All methods were also carried out in accordance with relevant guidelines and regulations with ethical permission from the Alexandria University Research Ethics Review Committee of the Faculty of Veterinary Medicine, Alexandria University (Approval No: Au/13/02/10/2023/015). In addition, approval was given by the University of Nottingham, School of Veterinary Medicine and Science Ethics Committee (No. 1843 160905), in accordance with institutional, national, and international guidelines.

## References

- Abd-Elhafeez HH, Kamal B, El-Sayed AM & Soliman SA (2021). MMP-9 expression in normal rabbit chondrocytes. *Cytol Histol Int J* 5(1), 1–9. <https://doi.org/10.23880/chij-16000131>
- Balah A, Bareedy MH, Abuel-Atta AA & Ghonimi W (2014). *Os cordis* of mature Dromedary camel heart (*Camelus dromedaries*) with



- special emphasis on *Cartilago cordis*. *J Adv Vet Anim Res* 1(3), 130. <https://doi.org/10.5455/javar.2014.a26>
- Barasa A & Gobetto A (1957). [The great *os cordis* of the bovines; histogenesis, structure and transformation according to age]. *Arch Biol (Liege)* 68(4), 541–560 passim.
- Best A, Egerbacher M, Swaine S, Pérez W, Alibhai A, Rutland P, Kubale V, El-Gendy SAA, Alsafy MAM, Baiker K, Sturrock CJ & Rutland CS (2022). Anatomy, histology, development and functions of *Ossa cordis*: A review. *Anat Histol Embryol* 51(6), 683–695. <https://doi.org/10.1111/ah.12861>
- Boersema S, da Silva J, Mee J & Noordhuizen J (2010). *Farm Health and Productivity Management of Dairy Young Stock*. Netherlands: Wageningen Academic Publishers.
- Bouxsein ML, Boyd SK, Christiansen BA, Guldberg RE, Jepsen KJ & Müller R (2010). Guidelines for assessment of bone microstructure in rodents using micro-computed tomography. *J Bone Miner Res* 25(7), 1468–1486. <https://doi.org/10.1002/jbmr.141>
- Chappard D, Baslé MF, Legrand E & Audran M (2011). New laboratory tools in the assessment of bone quality. *Osteoporos Int* 22(8), 2225–2240. <https://doi.org/10.1007/s00198-011-1573-6>
- Daetwyler HD, Capitan A, Pausch H, Stothard P, van Binsbergen R, Brøndum RF, Liao X, Djari A, Rodriguez SC, Grohs C, Esquerré D, Bouche O, Rossignol MN, Klopp C, Rocha D, Fritz S, Eggen A, Bowman PJ, Coote D, Chamberlain AJ, Anderson C, VanTassell CP, Hulsegge I, Goddard ME, Guldbbrandtsen B, Lund MS, Veerkamp RF, Boichard DA, Fries R & Hayes BJ (2014). Whole-genome sequencing of 234 bulls facilitates mapping of monogenic and complex traits in cattle. *Nat Genet* 46(8), 858–865. <https://doi.org/10.1038/ng.3034>
- Daghash S & Farghali H (2017). The cardiac skeleton of the Egyptian Water buffalo (*Bubalus bubalis*). *Int J Adv Res Biol Sci* 4(5), 1–13. <https://doi.org/10.22192/ijarbs.2017.04.05.001>
- Dankowski R, Baszko A, Sutherland M, Firek L, Kalmucki P, Wróblewska K, Szyszka A, Groothuis A & Siminiak T (2014). 3D heart model printing for preparation of percutaneous structural interventions: Description of the technology and case report. *Kardiol Pol* 72(6), 546–551. <https://doi.org/10.5603/KP.2014.0119>
- David T (1937). *Ossa cordis* of the carabao (*Bulbus bubalis*). *Philipp J Anim Ind* 4(6), 521–528.
- de Almeida Lima Massari CH, Ferreira-Silva A, Riceti-Magalhães HI, Souza-Silva DR & Miglino MA (2022). Computed tomography examination of the *os cordis* in a lamb (*Ovis aries Linnaeus*, 1758). *Revista MVZ Córdoba* 27(1), e2153. <https://doi.org/10.21897/rmvz.2153>
- Egerbacher M, Weber H & Hauer S (2000). Bones in the heart skeleton of the otter (*Lutra lutra*). *J Anat* 196(Pt 3)(Pt 3), 485–491. <https://doi.org/10.1046/j.1469-7580.2000.19630485.x>
- El-Bakary NER, Alsafy MAM, El-Gendy SAA & Elarab SME (2023). New insights into the retinal microstructure-diurnal activity relationship in the African five-lined skink (*Trachylepis quinquetaeniata*) (Lichtenstein, 1823). *Zoological Lett* 9(1), 7. <https://doi.org/10.1186/s40851-023-00205-w>
- El-Gendy SAA, Alsafy MAM, Rutland CS, Ez Elarab SM, Abd-Elhafeez HH & Kamal BM (2023). *Ossa cordis* and *os aorta* in the one-humped camel: Computed tomography, light microscopy and morphometric analysis. *Microsc Res Tech* 86(1), 53–62. <https://doi.org/10.1002/jemt.24256>
- Endo H, Sakai T, Itou T, Koie H & Kimura J (2005). Macroscopic observation and CT examination of the heart ventricular walls in the Asian elephant. *Mammal Study* 30(2), 125–130. [https://doi.org/10.3106/1348-6160\(2005\)30\[125:MOACEO\]2.0.CO;2](https://doi.org/10.3106/1348-6160(2005)30[125:MOACEO]2.0.CO;2)
- Frink RJ & Merrick B (1974). The sheep heart: Coronary and conduction system anatomy with special reference to the presence of an *os cordis*. *Anat Rec* 179(2), 189–200. <https://doi.org/10.1002/ar.1091790204>
- Gamble M (2008). 9—The Hematoxylin and Eosin. In *Theory and Practice of Histological Techniques (Sixth Edition)*, Bancroft JD & Gamble M (Eds.), pp. 121–134. Edinburgh: Churchill Livingstone.
- Gebert A & Preiss G (1998). A simple method for the acquisition of high-quality digital images from analog scanning electron microscopes. *J Microsc* 191(3), 297–302. <https://doi.org/10.1046/j.1365-2818.1998.00380.x>
- Habermehl K-H & Schmack K-H (1986). The topography at the level of the valves of the equine, bovine and canine hearts. *J Vet Med Ser C*.
- James TN (1965). Anatomy of the sinus node, AV node and *os cordis* of the beef heart. *Anat Rec* 153(4), 361–371. <https://doi.org/10.1002/ar.1091530405>
- James TN & Drake EH (1968). Sudden death in Doberman pinschers. *Ann Intern Med* 68(4), 821–829. <https://doi.org/10.7326/0003-4819-68-4-821>
- Junqueira LC, Bignolas G & Brentani RR (1979). Picrosirius staining plus polarization microscopy, a specific method for collagen detection in tissue sections. *Histochem J* 11(4), 447–455. <https://doi.org/10.1007/BF01002772>
- Keane M, Paul E, Sturrock CJ, Rauch C & Rutland CS (2017). Computed tomography in veterinary medicine: Currently published and tomorrow's vision. In *Computed Tomography—Advanced Applications*, Halefoğlu AM (Eds.), pp. 271–289. England: InTechOpen.
- Kuzela DC, Huffer WE, Conger JD, Winter SD & Hammond WS (1977). Soft tissue calcification in chronic dialysis patients. *Am J Pathol* 86(2), 403–424.
- Kytr D, Petranova V & Jirousek O (2012). Assessment of micromechanical properties of trabecular bone using quantitative backscattered electron microscopy. In 13th Bilateral Czech/German Symposium, pp. 119–122. Telč, Germany
- Lenstra JA & Bradley DG (1999). Systematics and phylogeny of cattle. In *The Genetics of Cattle*, Fries RE, Ruvinsky AO (Eds.), pp. 1–14. Oxon, UK: CABI Publishing.
- Long CA & Smart DL (1976). Variation and correlation of *os-cordis* and heart on *Odocoileus-virginianus* (Artiodactyla). *Tex J Sci* 27(1), 155–161.
- Maguigad MS & Balagan EJY (2021). Gross anatomy of the heart of mature Philippine water Buffalo (*Bubalus bubalis* L.). *CLSU Int J Sci Technol* 4(1), 10–23. <https://doi.org/10.22137/ijst.2021.v5n1.02>
- Matsuda K, Tabata S, Kawamura Y, Kurosawa T, Yoshie N & Taniyama H (2010). Ectopic ossification with haematopoietic bone marrow in the heart valves of a crossbred heavy horse. *J Comp Pathol* 143(2–3), 213–217. <https://doi.org/10.1016/j.jpca.2010.01.013>
- Mohammadpour AA (2007). Morphological study of the heart and *os cordis* in sheep and goat. *Indian Vet J* 84(3), 284–287.
- Moitié S, Baiker K, Strong V, Cousins E, White K, Liptovszky M, Redrobe S, Alibhai A, Sturrock CJ & Rutland CS (2020). Discovery of *os cordis* in the cardiac skeleton of chimpanzees (*Pan troglodytes*). *Sci Rep* 10(1), 9417. <https://doi.org/10.1038/s41598-020-66345-7>
- Molina-Flores B, Manzano-Baena P & Coulibaly MD (2020). *The Role of Livestock in Food Security, Poverty Reduction and Wealth Creation in West Africa*. Accra, Ghana: FAO.
- Moreira CA, Dempster DW & Baron R (2000). Anatomy and ultrastructure of bone—Histogenesis, growth and remodeling. In *Endotext*, Feingold KR, Anawalt B, Blackman MR, Boyce A, Chrousos G, Corpas E, de Herder WW (Eds.), pp. 2000–. South Dartmouth, MA: MDText.com, Inc.
- Morsy MA, Nigm AA, Mostageer A & Pirchner F (1984). Some economic characteristics of the Egyptian Baladi cattle. *Egypt J Anim Prod* 24(1–2), 273–286. <https://doi.org/10.21608/ejap.1984.128022>
- Nasoori A (2020). Formation, structure, and function of extra-skeletal bones in mammals. *Biol Rev* 95(4), 986–1019. <https://doi.org/10.1111/brv.12597>
- Pour A (2004). Comparative morphometry of the heart in Holstein and a native Iranian cow breeds with emphasis on the *os cordis*. *Indian Vet J (India)* 81(7), 806–809.



- Rühland C, Schönherr E, Robenek H, Hansen U, Iozzo RV, Bruckner P & Seidler DG (2007). The glycosaminoglycan chain of decorin plays an important role in collagen fibril formation at the early stages of fibrillogenesis. *FEBS J* 274(16), 4246–4255. <https://doi.org/10.1111/j.1742-4658.2007.05951.x>
- Rutland C (2021). *The Cow: A Natural and Cultural History*. Princeton, USA: Princeton University Press.
- Standing S (2016). *Gray's Anatomy: The Anatomical Basis of Clinical Practice*. Netherlands: Elsevier Limited.
- Steiner I, Kašparová P, Kohout A & Dominik J (2007). Bone formation in cardiac valves: A histopathological study of 128 cases. *Virchows Arch* 450(6), 653–657. <https://doi.org/10.1007/s00428-007-0430-7>
- Suvarna KS, Layton C & Bancroft JD (2018). *Bancroft's Theory and Practise of Histological Techniques*. Netherlands: Elsevier.
- Svensson L, Heinegård D & Oldberg A (1995). Decorin-binding sites for collagen type I are mainly located in leucine-rich repeats 4–5. *J Biol Chem* 270(35), 20712–20716. <https://doi.org/10.1074/jbc.270.35.20712>
- Tohno S, Azuma C, Tohno Y, Moriwake Y, Izu A, Kumai T & Minami T (2007). Increases of calcium, phosphorus, and magnesium in both the right and left fibrous trigones of human heart with aging. *Biol Trace Elem Res* 119, 111–119. <https://doi.org/10.1007/s12011-007-0053-5>
- Trainini J, Lowenstein J, Beraudo M, Wernicke M, Trainini A, Llabata V & Carreras C (2021). Myocardial torsion and cardiac fulcrum. *Morphologie* 105(348), 15–23. <https://doi.org/10.1016/j.morpho.2020.06.010>
- United Nations (2023). *Transboundary Breed: Holstein (Black and White)*. Domestic Animal Diversity Information System of the Food and Agriculture Organization of the United Nations. New York, USA: United Nations.
- Vazquez N, Dos Santos D, Pérez W, Artigas R & Sorriba V (2019). Gross anatomy of the heart of pampas deer (*Ozotoceros bezoarticus*, Linnaeus 1758). *J Morphol Sci* 36(3), 190–195. <https://doi.org/10.1055/s-0039-1692159>
- Witkowska A, Alibhai A, Hughes C, Price J, Klisch K, Sturrock CJ & Rutland CS (2014). Computed tomography analysis of Guinea pig bone: Architecture, bone thickness and dimensions throughout development. *Peer J* 2, e615. <https://doi.org/10.7717/peerj.615>
- Yoshida M, Miyoshi K, Tajima T, Wada A, Ueda H & Kooriyama T (2022). Anatomical features of *ossa cordis* in the Steller Sea lion. *J Vet Med Sci* 84(5), 660–665. <https://doi.org/10.1292/jvms.21-0261>
- Zhang K, Lenstra JA, Zhang S, Liu W & Liu J (2020). Evolution and domestication of the Bovini species. *Anim Genet* 51(5), 637–657. <https://doi.org/10.1111/age.12974>